

Rigorous verification of Hopf bifurcations via desingularization and continuation

Jan Bouwe van den Berg ^{*} Jean-Philippe Lessard [†] Elena Queirolo [‡]

June 25, 2020

Abstract

In this paper we present a general approach to rigorously validate Hopf bifurcations as well as saddle-node bifurcations of periodic orbits in systems of ODEs. By a combination of analytic estimates and computer-assisted calculations, we follow solution curves of cycles through folds, checking along the way that a single nondegenerate saddle-node bifurcation occurs. Similarly, we rigorously continue solution curves of cycles starting from their onset at a Hopf bifurcation. We use a blowup analysis to regularize the continuation problem near the Hopf bifurcation point. This extends the applicability of validated continuation methods to the mathematically rigorous computational study of bifurcation problems.

Keywords

Hopf bifurcation · continuation · desingularization · computer-assisted proofs

Mathematics Subject Classification (2010)

37G15 · 65P30 · 65G40 · 34C25 · 37C27

1 Introduction

In dynamical systems, bifurcations are of key importance to understand global parameter dependence of the dynamics. The analysis of bifurcations by pen and paper is generally restricted to cases where the solution at the bifurcation point is known analytically, and even in such cases it is often not feasible to examine properly the associated eigenvalue problem by hand. Hence numerical methods are applied ubiquitously to study bifurcation diagrams, for example using specialized software such as AUTO [7], MatCont [6], PyDSTool [4], XPP [8] and COCO [5]. This involves both the numerical continuation of solutions as well as the computational analysis of bifurcation points. To make such numerical simulations into rigorous mathematical statements, additional effort is required. For this purpose rigorous verification schemes (sometimes referred to as *a posteriori error analysis*) have been developed for a variety of continuation problems in the past decade, see [1, 3, 9, 26, 28, 29] and the references therein. The analogous methodology for bifurcation problems is much less developed, although some foundational results on pitchfork and saddle-node have been obtained in [1, 11, 17, 19, 30, 31, 32]. Moreover, double

^{*}Department of Mathematics, VU Amsterdam, 1081 HV Amsterdam, The Netherlands, janbouwe@few.vu.nl; partially supported by NWO-VICI grant 639033109.

[†]Department of Mathematics and Statistics, McGill University, 805 Sherbrooke St W, Montreal, QC, H3A 0B9, Canada, jp.lessard@mcgill.ca; supported by NSERC.

[‡]Department of Mathematics, Rutgers University, 110 Frelinghuysen Road, Piscataway, NJ 08854-8019, USA. elena.queirolo@rutgers.edu.

turning points [21, 24], period doubling bifurcations [31] and cocoon bifurcations [13] have also been considered.

In this paper we develop a general framework for the rigorous verification of Hopf bifurcations. We consider the class of polynomial vector fields

$$\dot{u} = f(u, \mu) \tag{1.1}$$

where $u \in \mathbb{R}^n$, $\mu \in \mathbb{R}$ represents the parameter in the system and $f : \mathbb{R}^n \times \mathbb{R} \rightarrow \mathbb{R}^n$ is polynomial both in u and μ . In our presentation, we choose the parameter μ to be one-dimensional, as generically it is the appropriate condition for curves of periodic orbits to exist. The polynomial dependence of f on u means that the estimates from [28] apply. We note that [28] includes an extensive discussion of the technical advantages that polynomial vector fields offer, as well as an array of generalizations. Indeed, the ideas in the current paper can be carried through for nonpolynomial vector fields, but that will require some supplemental effort. For example, by introducing new variables it is possible to transform a nonpolynomial vector field into a higher dimensional polynomial vector field (e.g. see [2, 12, 18]), and then apply a slight modification of the approach proposed in the current paper. Additionally, the presented approach can be extended to infinite dimensional dynamical systems described by delay-differential equations or parabolic partial differential equations, which is work in progress.

While our primary aim is the study of Hopf bifurcations, along the way we develop a technique to rigorously establish non-degeneracy of fold bifurcations for periodic orbits. Indeed, using a blowup strategy we convert the Hopf bifurcation problem into a regular continuation problem. A simpler version of this desingularization technique was already used in computationally analyzing the periodic solutions near the Hopf bifurcation in Wright's delay equation in [16], see also [25] for a similar but essentially analytic version. A fold in the associated continuation problem corresponds to a Hopf bifurcation in the original bifurcation problem.

The main contribution of this paper is a flexible and mathematically rigorous computational framework to study folds of periodic orbits and Hopf bifurcations in ODEs. In particular, the blowup technique allows computing a smooth global branch of periodic orbits starting from a Hopf bifurcation point. In future work we plan to adapt the blowup technique to other symmetry breaking bifurcations (e.g. pitchfork and period-doubling) yielding rigorous computations of global smooth branches of periodic orbits starting from such bifurcation points.

We now introduce the main ingredients of the paper, referring to subsequent sections for precise statements. Since in general the period L of the periodic solutions is a priori unknown and depends on the parameters, it is convenient to rescale time and add the (normalized) period $\tau = \frac{L}{2\pi}$ to the set of parameters $\lambda = (\tau, \mu) \in \mathbb{R}^2$ to arrive at the system

$$\begin{cases} \dot{u} = \tilde{f}(u, \lambda), \\ u \text{ is } 2\pi\text{-periodic}, \end{cases} \tag{1.2}$$

where the derivative is now with respect to the new time variable, and $\tilde{f}(u, \lambda) \stackrel{\text{def}}{=} \tau f(u, \mu)$.

We break the translation invariance of solutions to the autonomous problem by appending a phase condition. Moreover, to describe curves of solutions, it is expedient to introduce a ‘‘continuation’’ equation, depending on a continuation parameter s . Since we will work primarily in Fourier space, it is convenient to choose a phase condition which depends on the Fourier modes rather than coordinates in phase space. Hence we introduce \hat{u} to denote the Fourier coefficients of u . We note that without any essential loss of flexibility we restrict attention to phase and continuation equations that depend affine linearly on *finitely* many of the Fourier modes \hat{u} and λ only, while also the dependence on s may be affine linear. This leads to a system

$$\begin{cases} \dot{u} = \tilde{f}(u, \lambda), \\ \tilde{g}_s(\hat{u}, \lambda) = 0, \\ u \text{ is } 2\pi\text{-periodic}, \end{cases} \tag{1.3}$$

where $\tilde{g}_s \in \mathbb{R}^2$ represents the two (phase and continuation) appended equations just discussed. We expect to find curves of solutions to (1.3), parametrized by s , where both $u(t)$ and $\lambda = (\tau, \mu)$ are unknowns. In what follows, some additional “phase” conditions (to be specified later) will be absorbed into \tilde{g}_s , for example in order to break natural continuous symmetries.

For fixed s the problem (1.3) is expected to have isolated solutions, and we may move to Fourier space to set up a corresponding fixed point map. We do this in Section 2 and we reduce checking contractivity of this map in a ball of radius r (in some appropriately chosen Banach space) around a numerical approximation of a solution, to checking finitely many inequalities. All the bounds, parametrized by r , necessary to verify contractivity have been formulated in great generality in [28]. The verification of contraction can then be carried out with a computer based on interval arithmetic calculations. To obtain a curve of solutions we apply the uniform contraction principle, with explicit error bound given by the smallest $r = r_{\min}$ for which we can prove (uniform) contractivity. This parametrized Newton-Kantorovich methodology is explained in more detail in Section 2.

Given a bounded interval $I \subset \mathbb{R}$, to check that the solution curve $\{(u(t; s), \lambda(s))\}_{s \in I}$ (with $\lambda(s) = (\tau(s), \mu(s))$) has a nondegenerate fold (or saddle-node) bifurcation with respect to μ we need to find an $s_* \in I$ such that $\mu'(s_*) = 0$ and $\mu''(s_*) \neq 0$. To find the values of the s -derivative, we differentiate (1.3) twice with respect to s , and consider the derivatives to be part of the set of unknowns. We arrive at an extended system

$$\begin{cases} \dot{\mathbf{u}} = \tilde{\mathbf{f}}(\mathbf{u}, \boldsymbol{\lambda}), \\ \tilde{\mathbf{g}}_s(\dot{\mathbf{u}}, \boldsymbol{\lambda}) = 0, \\ \mathbf{u} \text{ is } 2\pi\text{-periodic,} \end{cases} \quad (1.4)$$

for $\mathbf{u}(t) \stackrel{\text{def}}{=} (u, u', u'')(t) \in \mathbb{R}^{3n}$ and $\boldsymbol{\lambda} \stackrel{\text{def}}{=} (\lambda, \lambda', \lambda'') \in \mathbb{R}^6$, where primes denote derivatives with respect to s . The extended $\tilde{\mathbf{f}}$ represents a vector field on \mathbb{R}^{3n} , and $\tilde{\mathbf{g}}_s(\dot{\mathbf{u}}, \boldsymbol{\lambda}) \in \mathbb{R}^6$ incorporates extended phase and continuation equations which depend affine linearly on finitely many of the Fourier modes $\dot{\mathbf{u}}$ and $\boldsymbol{\lambda}$, as well as affine linearly on s . We conclude that (1.4) is thus of the same form as (1.3), hence the continuation method from Section 2 and [28] still applies. We then use the rigorous error control r_{\min} to check that for some interval $[s_0, s_1]$ we have

$$\begin{cases} \mu'(s_0)\mu'(s_1) < 0 \\ |\mu''(s)| > 0, \quad \text{for all } s \in [s_0, s_1]. \end{cases}$$

This guarantees the existence of a single, nondegenerate fold bifurcation at some $s_* \in (s_0, s_1)$ along the curve $\{(u(t; s), \lambda(s))\}_{s \in [s_0, s_1]}$. The sign of the second derivative controls the direction of the fold. The details of this construction are presented in Section 3. In Section 4 we discuss the information which we can extract about the eigenvalue behaviour (and thus (in)stability of the periodic orbits).

To capture periodic orbits that bifurcate from an equilibrium at a Hopf bifurcation, we use a blowup procedure. We write $u(t) = y + a\bar{u}(t)$, where $y \in \mathbb{R}^n$ solves the equilibrium version of (1.3), and the “amplitude” $a \in \mathbb{R}$ is appended to the set of parameters, while simultaneously an additional “amplitude” condition, say $g_s^{\text{ampl}}(\hat{u}) = 0 \in \mathbb{R}$, is imposed, which embodies that \bar{u} is order 1. The amplitude condition function g_s^{ampl} depends again affine linearly on finitely many Fourier modes.

Since $y \in \mathbb{R}^n$ is a time-independent equilibrium solution, it also gets appended to the set of parameters:

$$\bar{\boldsymbol{\lambda}} \stackrel{\text{def}}{=} (\tau, a, y, \mu) \in \mathbb{R}^{3+n},$$

and correspondingly

$$\bar{g}_s(\hat{u}, \bar{\boldsymbol{\lambda}}) \stackrel{\text{def}}{=} (\tilde{g}_s^{\text{phase}}(\hat{u}), g_s^{\text{ampl}}(\hat{u}), f(y, \mu), \tilde{g}_s^{\text{cont}}(\hat{u}, \bar{\boldsymbol{\lambda}})) \in \mathbb{R}^{3+n},$$

where $\tilde{g}_s^{\text{phase}} = 0$ and $\tilde{g}_s^{\text{cont}} = 0$ denote the phase condition and continuation equation, respectively.

The ODE for $\bar{u}(t) \in \mathbb{R}^n$ is given by

$$\dot{\bar{u}} = \bar{f}(\bar{u}, \bar{\lambda}) \stackrel{\text{def}}{=} \begin{cases} \frac{\tilde{f}(y + a\bar{u}, \lambda) - \tilde{f}(y, \lambda)}{a} & \text{if } a \neq 0, \\ D_u \tilde{f}(y, \lambda) \bar{u} & \text{if } a = 0, \end{cases} \quad (1.5)$$

which represents a rescaled smooth vector field, and \bar{f} is polynomial if \tilde{f} is. The new *desingularized Hopf problem*

$$\begin{cases} \dot{\bar{u}} = \bar{f}(\bar{u}, \bar{\lambda}), \\ \bar{g}_s(\bar{u}, \bar{\lambda}) = 0, \\ \bar{u} \text{ is } 2\pi\text{-periodic,} \end{cases} \quad (1.6)$$

is then again of the form (1.3), hence the continuation machinery from Section 2 and [28] is directly applicable. This leads to continuation of periodic solution “through” the Hopf bifurcation at $a = 0$. In order to show that the Hopf bifurcation is nondegenerate, and to determine its direction, the saddle-node construction (1.4) is then applied to (1.6). More precisely, this leads to the extended system

$$\begin{cases} \dot{\bar{u}} = \bar{f}(\bar{u}, \bar{\lambda}), \\ \bar{g}_s(\bar{u}, \bar{\lambda}) = 0, \\ \bar{u} \text{ is } 2\pi\text{-periodic,} \end{cases} \quad (1.7)$$

for $\bar{u}(t) = (\bar{u}, \bar{u}', \bar{u}'')(t) \in \mathbb{R}^{3n}$ and $\bar{\lambda} = (\bar{\lambda}, \bar{\lambda}', \bar{\lambda}'') \in \mathbb{R}^{3(3+n)}$, where primes denote derivatives with respect to s . The details of this construction are given in Section 5. When continuing a branch of periodic orbits that originates from a Hopf bifurcation far away from the bifurcation point, one would like to switch back from the desingularized formulation (1.6) to the original system (1.2). This topic is discussed briefly in Section 6.

To illustrate our approach with an example, consider the extended Lorenz-84 system [14, 15]

$$\begin{cases} \dot{u}_1 = -u_2^2 - u_3^2 - \xi_1 u_1 - \xi_1 \xi_6 - \xi_2 u_4^2, \\ \dot{u}_2 = u_1 u_2 - \xi_3 u_1 u_3 - u_2 + \xi_4, \\ \dot{u}_3 = \xi_3 u_1 u_2 + u_1 u_3 - u_3, \\ \dot{u}_4 = -\xi_5 u_4 + \xi_2 u_4 u_1 + \mu, \end{cases} \quad (1.8)$$

which has a four dimensional phase space and seven parameters. In Figure 1 we depict a full continuous branch of periodic orbits of (1.8) with μ as the “continuation” parameter, starting at one Hopf bifurcation point and finishing at another one. The two equilibria with Hopf bifurcation points, which are connected by this branch of periodic solutions, lie on different continuation curves, i.e., the periodic orbits “cross over” from one branch of equilibria to another. Further details are discussed in Section 7.2.

Several other examples of fold and Hopf bifurcations are also presented in Section 7. This includes an illustration in Section 7.4 of how Hamiltonian systems, which are very nongeneric from the point of view of periodic orbits, can nevertheless be analyzed using the methods in the current paper. The accompanying MATLAB code can be found at [27].

2 Setup for the continuation of periodic orbits in Fourier space

We briefly introduce the setup of the continuation problems under consideration in this paper. Additional details can be found in [28]. Consider a polynomial vector field of the form

$$\begin{cases} \dot{u} = h(u, \lambda), \\ g(\lambda) = 0, \\ u \text{ is } 2\pi\text{-periodic,} \end{cases} \quad (2.1)$$

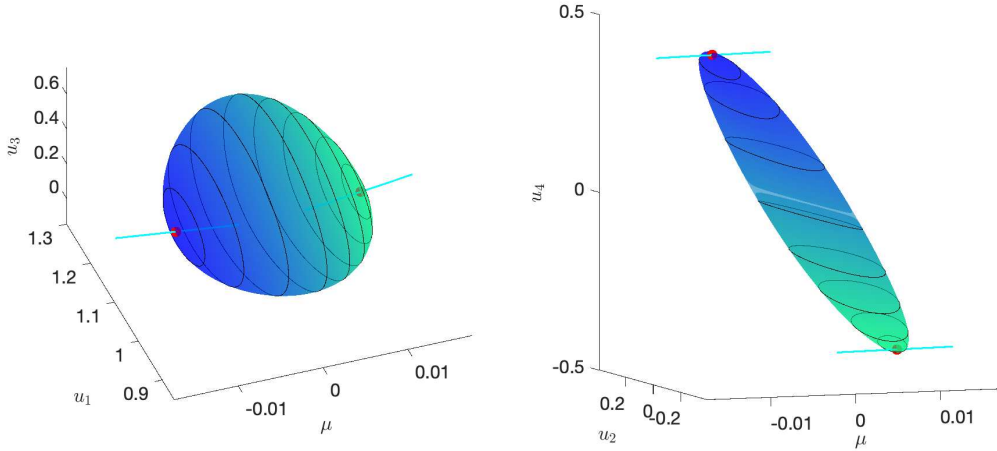


Figure 1: A branch of periodic solutions of system (1.8) with varying μ and fixed parameters $(\xi_1, \xi_2, \xi_3, \xi_4, \xi_5, \xi_6) = (0.25, 0.987, 1, 0.25, 1.04, 2)$. Validated continuation combined with gluing (see Section 6) proves the existence of such a *balloon* of periodic orbits, connecting two equilibria (red dots) undergoing the Hopf bifurcations at different parameter values. These two equilibria are not connected by continuation at the level of stationary states, nor related by symmetry, see Section 7.2 for more details. The branches of the equilibria undergoing the Hopf bifurcations are plotted in cyan. The balloon is colored by μ -value.

where $h : \mathbb{R}^n \times \mathbb{R}^m \rightarrow \mathbb{R}^n$ is a polynomial vector field and $g : \mathbb{R}^m \rightarrow \mathbb{R}^{m'}$ is a polynomial mapping. The maps h and g depend on the problem under study. For the standard *pseudo-arclength* continuation of periodic orbits, $m = 2$, $m' = 0$, $\lambda = (\tau, \mu) \in \mathbb{R}^2$, $h = \tilde{f} : \mathbb{R}^n \times \mathbb{R}^2 \rightarrow \mathbb{R}^n$ is defined in (1.2) and $g \equiv 0$. For the continuation of periodic orbits passing through a Hopf bifurcation, $m = 3 + n$, $m' = n$, $\lambda = (\tau, a, y, \mu) \in \mathbb{R}^{3+n}$, $h = \tilde{f} : \mathbb{R}^n \times \mathbb{R}^{3+n} \rightarrow \mathbb{R}^n$ is defined in (1.5) and $g(\lambda) = f(y, \mu)$.

Remark 2.1. For the *pseudo-arclength* continuation, $g \equiv 0$ and therefore two equations are “missing” to balance the variable $\lambda \in \mathbb{R}^2$. In this case a phase condition and a continuation equation are appended. For the *desingularized Hopf* problem, three equations are missing as $\lambda \in \mathbb{R}^{3+n}$ is variable and $g(\lambda) = 0 \in \mathbb{R}^n$. A phase condition, a continuation equation and an amplitude equation are then introduced.

2.1 Formulation in Fourier space

We write the Fourier expansion of a 2π -periodic function $u = (u_1, \dots, u_n) : \mathbb{R} \rightarrow \mathbb{R}^n$ as

$$u(t) = \sum_{k \in \mathbb{Z}} (v)_k e^{ikt}, \quad (v)_k = (v_1, \dots, v_n)_k \in \mathbb{C}^n. \quad (2.2)$$

The differential equation $\dot{u} = h(u, \lambda) \in \mathbb{R}^n$ then transforms in Fourier space to

$$(F_i(x))_k \stackrel{\text{def}}{=} ik(v_i)_k - (\hat{h}_i(v, \lambda))_k = 0 \quad \text{for } 1 \leq i \leq n, k \in \mathbb{Z}, \quad (2.3)$$

where \hat{h}_i is the polynomial h_i , but with multiplications interpreted as convolutions, denoted

$$(\tilde{v}\tilde{v}')_k \stackrel{\text{def}}{=} \sum_{k' \in \mathbb{Z}} \tilde{v}_{k'} \tilde{v}'_{k-k'}.$$

To fix a Banach space in which we will apply contraction arguments, we introduce the ν -norm ($\nu \geq 1$) on $\mathbb{C}^{\mathbb{Z}}$ as

$$\|\tilde{v}\|_{\nu} \stackrel{\text{def}}{=} \sum_{k \in \mathbb{Z}} |\tilde{v}_k| \nu^{|k|}, \quad (2.4)$$

with corresponding Banach space $\ell_{\nu}^1 \stackrel{\text{def}}{=} \{\tilde{v} \in \mathbb{C}^{\mathbb{Z}} : \|\tilde{v}\|_{\nu} < \infty\}$. The space of variables $x = (v, \lambda)$ is then $X = X_{\nu} \stackrel{\text{def}}{=} (\ell_{\nu}^1)^n \times \mathbb{C}^m$. On the components of $x = (x_1, \dots, x_{m+n}) = (v_1, \dots, v_n, \lambda_1, \dots, \lambda_m)$ we define the norm

$$\|x_j\| \stackrel{\text{def}}{=} \begin{cases} \|x_j\|_{\nu} & \text{for } 1 \leq j \leq n, \\ |x_j| & \text{for } n+1 \leq j \leq n+m, \end{cases}$$

leading to the product norm

$$\|x\|_X \stackrel{\text{def}}{=} \max_{1 \leq j \leq m+n} \|x_j\|. \quad (2.5)$$

We introduce the time derivative on ℓ_{ν}^1 by

$$(\text{iK}\tilde{v})_k \stackrel{\text{def}}{=} \text{i}k\tilde{v}_k, \quad \text{for } k \in \mathbb{Z},$$

which we extend to X via $\text{iK}x = (\text{iK}v_1, \dots, \text{iK}v_n, 0, \dots, 0)$.

Finite dimensional numerical approximations are found in the truncated space

$$X_K \stackrel{\text{def}}{=} \{x = (v, \lambda) \in X : (v_i)_k = 0 \text{ for all } |k| > K, 1 \leq i \leq n\}$$

for some $K \in \mathbb{N}$. The space X_K can be identified with $\mathbb{C}^{m+n(2K+1)}$ and it will be convenient notationally to introduce the following bilinear form on X_K :

$$\langle x, x' \rangle \stackrel{\text{def}}{=} \sum_{i=1}^n \sum_{k=-K}^K (v_i)_k (v'_i)_k + \sum_{j=1}^m \lambda_j \lambda'_j. \quad (2.6)$$

In order to recover a real-valued solution we will check a posteriori that $(v_i)_{-k} = \overline{(v_i)_k}$ using equivariance of the problem under the conjugation symmetry defined below.

Definition 2.2. *The conjugate $x^* = (v^*, \lambda^*)$ of $x = (v, \lambda) \in X$ is given by*

$$\lambda_j^* = \overline{\lambda_j} \text{ for } 1 \leq j \leq m, \quad (v_i^*)_k = \overline{(v_i)_{-k}} \text{ for } 1 \leq i \leq n, k \in \mathbb{Z}.$$

The set of conjugate symmetric elements is denoted by $\mathcal{S} = \{x \in X : x^ = x\}$, and $\mathcal{S}_K = \mathcal{S} \cap X_K$.*

We note that both F and g are equivariant under the conjugation symmetry: $F(x^*) = F(x)^*$ and $g(\lambda^*) = g(\lambda)^*$. Note that the equivariance of g follows from the fact that it is a real polynomial mapping. Furthermore, $\langle x, x' \rangle \in \mathbb{R}$ for $x, x' \in \mathcal{S}_K$.

To set up the rigorous continuation framework, let us assume we have two points $\hat{x}_0 = (\hat{v}_0, \hat{\lambda}_0) \in \mathcal{S}_K$ and $\hat{x}_1 = (\hat{v}_1, \hat{\lambda}_1) \in \mathcal{S}_K$ which each represent an approximate solution of

$$\begin{cases} F(x) = 0, \\ g(\lambda) = 0. \end{cases} \quad (2.7)$$

We define the interpolation

$$\hat{x}_s = (\hat{v}_s, \hat{\lambda}_s) \stackrel{\text{def}}{=} (1-s)\hat{x}_0 + s\hat{x}_1 \quad \text{for } s \in [0, 1].$$

To introduce the phase condition we define $q^{\mathcal{C}} = (q_v^{\mathcal{C}}, 0) \in \mathcal{S}_K$ with

$$(q_v^{\mathcal{C}})_j = \overline{\text{iK}(\hat{v}_{\frac{1}{2}})_j} \quad \text{for } |k| \leq K, 1 \leq j \leq n. \quad (2.8)$$

We choose the phase condition

$$G^{\mathbb{C}}(x) \stackrel{\text{def}}{=} \langle q^{\mathbb{C}}, x \rangle = 0.$$

This phase equation does not depend on s , which deviates slightly from the one in [28]. Having an s -dependent phase condition is convenient when validating long stretches of a solution branch (essentially, it assists in “gluing” short pieces into a long smooth curve). Here we are interesting in verifying a solution branch near a bifurcation point, hence s -dependence is not necessary and merely complicates the algebra and notation.

Remark 2.3. *We note that $G^{\mathbb{C}}$ depends linearly on x . Furthermore, $G^{\mathbb{C}}$ only depends on the Fourier coefficients with indices $|k| \leq K$. We will encounter slightly more general dependence for more general “phase” equations throughout, namely we allow for affine linear dependence on x and affine linear dependence on s . For this purpose we introduce the notation*

$$\mathcal{G}_{\psi_0, \psi_1}^{\phi_0, \phi_1}(x, s) \stackrel{\text{def}}{=} \langle (1-s)\phi_0 + s\phi_1, x \rangle - [(1-s)\psi_0 + s\psi_1], \quad (2.9)$$

for $\phi_0, \phi_1 \in \mathcal{S}_K$ and $\psi_0, \psi_1 \in \mathbb{R}$. In this notation $G^{\mathbb{C}}(x) = \mathcal{G}_{0,0}^{q^{\mathbb{C}}, q^{\mathbb{C}}}(x, s)$. We note that

$$\mathcal{G}_{\psi_0, \psi_1}^{\phi_0, \phi_1}(x^*, s) = \overline{\mathcal{G}_{\psi_0, \psi_1}^{\phi_0, \phi_1}(x, s)}.$$

Remark 2.4. *In case $h = \bar{f} : \mathbb{R}^{3+n} \times \mathbb{R}^n \rightarrow \mathbb{R}^n$ is the desingularized Hopf problem defined in (1.5), an extra phase-like condition is appended to the system, namely the (s -independent) amplitude equation*

$$G^{\oplus}(x) \stackrel{\text{def}}{=} \langle q^{\oplus}, x \rangle - 1 = \mathcal{G}_{1,1}^{q^{\oplus}, q^{\oplus}}(x, s) = 0,$$

where $q^{\oplus} = (q_v^{\oplus}, 0) \in \mathcal{S}_K$, with

$$(q_v^{\oplus})_i = \overline{\mathbb{K}^2(\hat{v}_{\frac{1}{2}})_i} \quad \text{for } |k| \leq K, 1 \leq i \leq n.$$

See Section 5 for more details and a motivation for this choice.

In an analogous manner we introduce an s -dependent continuation equation $G_s^{\odot}(x) = 0$. Indeed, we determine numerically “predictors” $\hat{x}_s \in \mathcal{S}_K$ of the tangent direction of the solution curve (for the problem including the phase condition) at \hat{x}_s for $s = 0, 1$. We set

$$q_s^{\odot} = \overline{\hat{x}_s},$$

so that $q_s^{\odot} \in \mathcal{S}_K$, and we define

$$\begin{aligned} G_s^{\odot}(x) &\stackrel{\text{def}}{=} \langle (1-s)q_0^{\odot} + sq_1^{\odot}, x \rangle - [(1-s)\langle q_0^{\odot}, \hat{x}_0 \rangle + s\langle q_1^{\odot}, \hat{x}_1 \rangle] \\ &= \mathcal{G}_{\langle q_0^{\odot}, \hat{x}_0 \rangle, \langle q_1^{\odot}, \hat{x}_1 \rangle}^{q_0^{\odot}, q_1^{\odot}}(x, s), \end{aligned} \quad (2.10)$$

hence the dependence of G^{\odot} on x and s is as described in Remark 2.3.

The full set of “algebraic” equations is

$$G_s(x) = \begin{bmatrix} G^{\mathbb{C}}(x) \\ G_s^{\odot}(x) \end{bmatrix} \quad \text{or} \quad G_s(x) = \begin{bmatrix} G^{\mathbb{C}}(x) \\ G^{\oplus}(x) \\ g(\lambda) \\ G_s^{\odot}(x) \end{bmatrix},$$

for the pseudo-arclength continuation and the desingularized Hopf problem, respectively. The general zero finding problem for continuation is

$$H_s(x) \stackrel{\text{def}}{=} \begin{bmatrix} F(x) \\ G_s(x) \end{bmatrix} = 0. \quad (2.11)$$

Clearly, conjugate symmetric zeros of H_s correspond to periodic orbits of (1.1), provided $\tau = \lambda_1 \neq 0$.

We define the associated fixed point operator

$$T_s(x) \stackrel{\text{def}}{=} x - A_s H_s(x), \quad T_s : X \rightarrow X, \quad s \in [0, 1]. \quad (2.12)$$

Here A_s is an injective map that approximates the inverse of the Jacobian $D_x H_s(\hat{x}_s)$. We do not elaborate on the choice for A_s , which is discussed in detail in [28, Section 8.2]. For the current discussion it suffices to say that $A_s = (1 - s)A_0 + sA_1$, and A_s , $\mathbf{s} = 0, 1$ are approximate inverses of the Jacobians at the end points \hat{x}_s . Each linear operator A_s , $\mathbf{s} = 0, 1$ is made up from a $(m + n(2K + 1)) \times (m + n(2K + 1))$ matrix and a diagonal infinite tail. In particular, let Π_K denote the natural projection of X onto X_K , then the block structure (finite matrix and infinite tail) of A_s is characterized by $A_s \Pi_K = \Pi_K A_s$ and $A_s(I - \Pi_K) = (I - \Pi_K)A_s$, while the diagonal tail is given by

$$(I - \Pi_K)A_s x = (I - \Pi_K)(-iK^{-1}v_1, \dots, -iK^{-1}v_n, 0, \dots, 0),$$

with $(K^{-1}\tilde{v})_k \stackrel{\text{def}}{=} k^{-1}\tilde{v}_k$ for any $k \neq 0$. With regards to conjugation symmetry, the choice of A_s is such that $A_s x^* = (A_s x)^*$, hence $T_s(x^*) = T_s(x)^*$ for all $s \in [0, 1]$.

Let $B_r(x) \stackrel{\text{def}}{=} \{x' \in X : \|x - x'\|_X \leq r\}$, then the ‘‘tube’’ around the numerical line segment $\{\hat{x}_s : s \in [0, 1]\}$ is given by

$$\mathcal{C}_r \stackrel{\text{def}}{=} \bigcup_{s \in [0, 1]} B_r(\hat{x}_s). \quad (2.13)$$

In [28, Sections 6 and 8] explicitly computable bounds $Y = (Y_1, \dots, Y_{m+n})$ and $Z(r) = (Z_1, \dots, Z_{m+n})(r)$ are derived, that satisfy

$$Y_j \geq \max_{s \in [0, 1]} \|(T_s(\hat{x}_s) - \hat{x}_s)_j\|, \quad (2.14a)$$

$$Z_j(r) \geq \max_{s \in [0, 1]} \sup_{b, c \in B_1(0)} \|[D_x T_s(\hat{x}_s + rb)rc]_j\|, \quad (2.14b)$$

for $j = 1, \dots, m + n$. The following theorem, which is itself based on the uniform contraction principle (see for example [26, 3, 9] for similar results), is the crux of rigorously verified continuation.

Theorem 2.5 (Theorems 3.1 and 4.2 in [28]). *Assume Y and $Z(r)$ satisfy (2.14). Assume moreover that A_s is injective for all $s \in [0, 1]$. If there exists an $\hat{r} > 0$ such that*

$$Y_j + Z_j(\hat{r}) - \hat{r} < 0 \quad \text{for all } j = 1, \dots, m + n, \quad (2.15)$$

then T_s is a contraction on $B_{\hat{r}}(\hat{x}_s)$ for every s in $[0, 1]$. The fixed points $\hat{x}(s)$ of T_s in $B_{\hat{r}}(\hat{x}_s)$ are conjugate symmetric and form a continuous parametrized curve $\hat{x} : [0, 1] \rightarrow X$ in $\mathcal{C}_{\hat{r}}$, such that $H_s(\hat{x}(s)) = 0$ for every $s \in [0, 1]$.

Remark 2.6. *Injectivity of A_s follows by a computational check on the finite part, since invertibility of its diagonal tail is trivial to establish. For the implementation of the Z -bound chosen in [28], the former computational check is in fact implied by $Z(\hat{r}) < \hat{r}$, see [28, Section 8.5]. Since $\hat{x}(s) \in B_{\hat{r}}(\hat{x}_s)$, it follows from the inequalities (2.15) and the definition of the Z -bound (2.14b) that*

$$\|I - A_s D_x H_s(\hat{x}(s))\|_{B(X)} < 1,$$

where $\|\cdot\|_{B(X)}$ is the bounded linear operator norm on X . Hence $D_x H_s(\hat{x}(s))$ is injective.

3 Saddle-node bifurcation

It is computationally straightforward to check that the parametrized solution curve $\{\hat{x}(s)\}_{s \in [0,1]}$ is smooth, for example based on [28, Lemma 3.3], see also [3, 26]. Indeed, we need to check (computationally, using interval arithmetic) that

$$\hat{r} \langle q_1^\circ - q_0^\circ, b \rangle \neq \langle (1-s)q_1^\circ + sq_0^\circ, \hat{x}_1 - \hat{x}_0 \rangle \quad \text{for any } s \in [0,1] \text{ and } b \in B_1(0), \quad (3.1)$$

which in practice is satisfied since $\hat{x}_0 = \overline{q_0^\circ}$ and $\hat{x}_1 = \overline{q_1^\circ}$ are both almost parallel to $\hat{x}_1 - \hat{x}_0$, and $\hat{r} \ll 1$.

From now on we assume that Inequality (3.1) is satisfied. Since it implies that

$$D_s G_s^\circ(x) \neq 0 \quad \text{for any } x \in \mathcal{C}_{\hat{r}}, \quad (3.2)$$

we in particular obtain that $\hat{x}'(s) \neq 0$. Namely, let $\{x(s) = (1-s)\hat{x}_0 + s\hat{x}_1 + \hat{r}b(s)\}_{s \in [0,1]}$ with $b(s) \in B_1(0)$ be any smooth parametrized curve solving $G_s^\circ(x(s)) = 0$. Then, by formally differentiating the latter identity, we arrive, after some rearrangement of terms, at

$$\langle (1-s)q_1^\circ + sq_0^\circ, x'(s) \rangle = \hat{r} \langle q_0^\circ - q_1^\circ, b \rangle + \langle (1-s)q_1^\circ + sq_0^\circ, \hat{x}_1 - \hat{x}_0 \rangle.$$

Therefore, Inequality (3.1) implies the derivative $\hat{x}'(s)$, which exists since the curve is obtained through the uniform contraction principle (see e.g. [3, 26]), cannot vanish, and the curve is smooth. Since $G_s^\circ(\hat{x}(s)) = 0$ for all $s \in [0,1]$, and the inequality (3.2) implies that for any fixed $x \in \mathcal{C}_{\hat{r}}$ the function $[0,1] \ni s \mapsto G_s^\circ(x)$ vanishes at most once, all points in $\{x(s)\}_{s \in [0,1]}$ are distinct, hence the curve does not selfintersect (i.e. it is a smooth embedding).

Definition 3.1. The solution curve has a *nondegenerate fold bifurcation* with respect to some parameter λ_j if there is an $s_\star \in (0,1)$ such that

$$\dot{\lambda}_j'(s_\star) = 0 \quad \dot{\lambda}_j''(s_\star) \neq 0. \quad (3.3)$$

In this section we explain how to establish such nondegenerate folds. Note that we do not impose any eigenvalue restrictions in the description (3.3) of a nondegenerate fold. Considerations about eigenvalues and exchange of stability are discussed in Section 4.

Remark 3.2. We allow for any of the elements of the vector λ to be interpreted as the bifurcation parameter. Of course, the obvious choice is to take the original parameter μ in (1.1) as the bifurcation parameter. In some cases (e.g. Hamiltonian systems, boundary value problems) it may also be of interest to consider the normalized period τ as the bifurcation parameter, see Remark 5.2 and the example in Section 7.4.

To obtain equations for the derivatives $\hat{x}'(s)$ and $\hat{x}''(s)$, recall (2.11) and differentiate $H_s(\hat{x}(s))$ formally to obtain

$$H_s(\mathbf{x}^{[0]}) = 0, \quad (3.4a)$$

$$D_x H_s(\mathbf{x}^{[0]})\mathbf{x}^{[1]} + D_s H_s(\mathbf{x}^{[0]}) = 0, \quad (3.4b)$$

$$D_x H_s(\mathbf{x}^{[0]})\mathbf{x}^{[2]} + 2D_s D_x H_s(\mathbf{x}^{[0]})\mathbf{x}^{[1]} + D_x^2 H_s(\mathbf{x}^{[0]})\mathbf{x}^{[1]}, \mathbf{x}^{[1]} = 0, \quad (3.4c)$$

where we have used that $D_s^2 H_s(x)$ vanishes. The system (3.4) is solved by

$$(\mathbf{x}^{[0]}, \mathbf{x}^{[1]}, \mathbf{x}^{[2]})(s) = (\hat{x}(s), \hat{x}'(s), \hat{x}''(s)).$$

Remark 3.3. When $\mathbf{x}^{[0]} = \hat{x}(s)$ solves (3.4a), then the unique solutions of (3.4b) and (3.4c) are $(\mathbf{x}^{[1]}, \mathbf{x}^{[2]}) = (\hat{x}'(s), \hat{x}''(s))$, provided $D_x H_s(\mathbf{x}^{[0]}(s))$ is an injective linear operator. Remark 2.6 explains that this injectivity holds whenever we have found our solutions through Theorem 2.5, see also Remark 3.5.

We now show that the extended system is again of the general form (2.11), that is, finitely many algebraic equations and generalized phase equations with structure as described in Remark 2.3, and a polynomial vector field in Fourier space variables. Hence we can apply the construction of Theorem 2.5 to find solutions of (3.4).

We introduce $\mathbf{x} = (\mathbf{v}, \boldsymbol{\lambda}) \in (\ell_\nu^1)^{3n} \times \mathbb{C}^{3m} = \mathbf{X} \equiv X^3$, which we also represent as $\mathbf{x} = (\mathbf{x}^{[0]}, \mathbf{x}^{[1]}, \mathbf{x}^{[2]})$, with $\mathbf{x}^{[i]} = (\mathbf{v}^{[i]}, \boldsymbol{\lambda}^{[i]}) \in X$ for $i = 0, 1, 2$. The extended vector field $\mathbf{h}(\mathbf{u}, \boldsymbol{\lambda}) \in \mathbb{R}^{3n}$ of h given in (2.1) with $\boldsymbol{\lambda} = (\boldsymbol{\lambda}^{[0]}, \boldsymbol{\lambda}^{[1]}, \boldsymbol{\lambda}^{[2]}) \in \mathbb{R}^{3m}$ and $\mathbf{u} = (\mathbf{u}^{[0]}, \mathbf{u}^{[1]}, \mathbf{u}^{[2]}) \in \mathbb{R}^{3n}$ is defined by

$$\mathbf{h}(\mathbf{u}, \boldsymbol{\lambda}) \stackrel{\text{def}}{=} \begin{bmatrix} h(\mathbf{u}^{[0]}, \boldsymbol{\lambda}^{[0]}) \\ D_\lambda h(\mathbf{u}^{[0]}, \boldsymbol{\lambda}^{[0]})\boldsymbol{\lambda}^{[1]} + D_u h(\mathbf{u}^{[0]}, \boldsymbol{\lambda}^{[0]})\mathbf{u}^{[1]} \\ \mathbf{h}^{[2]}(\mathbf{u}, \boldsymbol{\lambda}) \end{bmatrix}, \quad (3.5)$$

where

$$\begin{aligned} \mathbf{h}^{[2]}(\mathbf{u}, \boldsymbol{\lambda}) \stackrel{\text{def}}{=} & D_\lambda^2 h(\mathbf{u}^{[0]}, \boldsymbol{\lambda}^{[0]})[\boldsymbol{\lambda}^{[1]}, \boldsymbol{\lambda}^{[1]}] + D_\lambda h(\mathbf{u}^{[0]}, \boldsymbol{\lambda}^{[0]})\boldsymbol{\lambda}^{[2]} \\ & + D_u^2 h(\mathbf{u}^{[0]}, \boldsymbol{\lambda}^{[0]})[\mathbf{u}^{[1]}, \mathbf{u}^{[1]}] + D_u h(\mathbf{u}^{[0]}, \boldsymbol{\lambda}^{[0]})\mathbf{u}^{[2]} \\ & + 2D_\lambda D_u h(\mathbf{u}^{[0]}, \boldsymbol{\lambda}^{[0]})[\boldsymbol{\lambda}^{[1]}, \mathbf{u}^{[1]}]. \end{aligned}$$

Similarly, the algebraic equations $g(\boldsymbol{\lambda}) = 0$ given in (2.1) are extended to

$$\mathbf{g}(\boldsymbol{\lambda}) = \begin{bmatrix} g(\boldsymbol{\lambda}^{[0]}) \\ D_\lambda g(\boldsymbol{\lambda}^{[0]})\boldsymbol{\lambda}^{[1]} \\ D_\lambda g(\boldsymbol{\lambda}^{[0]})\boldsymbol{\lambda}^{[2]} + D_\lambda^2 g(\boldsymbol{\lambda}^{[0]})[\boldsymbol{\lambda}^{[1]}, \boldsymbol{\lambda}^{[1]}] \end{bmatrix}.$$

For any phase condition of the form $\mathcal{G}_{\psi_0, \psi_1}^{\phi_0, \phi_1}(\mathbf{x}, s)$, see (2.9), the three extended equations are

$$\begin{aligned} \mathcal{G}_{\psi_0, \psi_1}^{(\phi_0, 0, 0), (\phi_1, 0, 0)}(\mathbf{x}, s) &= 0, \\ \mathcal{G}_{\psi_1 - \psi_0, \psi_1 - \psi_0}^{(\phi_1 - \phi_0, \phi_0, 0), (\phi_1 - \phi_0, \phi_1, 0)}(\mathbf{x}, s) &= 0, \\ \mathcal{G}_{0, 0}^{(0, 2(\phi_1 - \phi_0), \phi_0), (0, 2(\phi_1 - \phi_0), \phi_1)}(\mathbf{x}, s) &= 0. \end{aligned}$$

We note that each of these is of the form $\mathcal{G}_{\tilde{\psi}_0, \tilde{\psi}_1}^{\phi_0, \phi_1}(\mathbf{x}, s)$ with $\phi_s \in \mathbf{X}$ for $s \in \{0, 1\}$ such that $\phi_s^* = \phi_s$ and $\tilde{\psi}_s \in \mathbb{R}$, as described in Remark 2.3. Hence each of these is conjugate equivariant.

We collect all algebraic and extended phase condition equations in $\mathbf{G}_s(\mathbf{x})$. Since taking the Fourier transform and taking the derivative with respect to s commute, the system

$$\mathbf{H}_s(\mathbf{x}) \stackrel{\text{def}}{=} \begin{bmatrix} \mathbf{G}_s(\mathbf{x}) \\ \mathbf{F}(\mathbf{x}) \end{bmatrix} = 0$$

is equivalent to (3.4). Hence we may indeed apply the continuation technique (and code) from [28] as outlined in Section 2. Denote by $(\hat{\mathbf{x}}^{[0]}(s), \hat{\mathbf{x}}^{[1]}(s), \hat{\mathbf{x}}^{[2]}(s))$ the resulting solution curve for $s \in [0, 1]$.

Remark 3.4. *When applying the fixed point construction of Section 2, we need to choose an approximate inverse \mathbf{A}_s of the Jacobian. Since $D_{\mathbf{x}}\mathbf{H}_s(\mathbf{x})$ is block lower triangular with respect to the splitting $\mathbf{x} = (\mathbf{x}^{[0]}, \mathbf{x}^{[1]}, \mathbf{x}^{[2]})$, we will always select \mathbf{A}_s to be block lower triangular as well. This implies that if \mathbf{T}_s is a contraction on $\mathbf{X} = X^3$, then the restriction $\mathbf{T}_s^{[0]}(\mathbf{x}^{[0]})$ of $\mathbf{T}_s(\mathbf{x})$ to the first of the three components is well-defined and a contraction on X . Analogously, the map $(\mathbf{T}_s^{[0]}(\mathbf{x}^{[0]}), \mathbf{T}_s^{[1]}(\mathbf{x}^{[0]}, \mathbf{x}^{[1]}))$ is a contraction on X^2 .*

Remark 3.5. Since $D_{\mathbf{x}}\mathbf{H}_s(\mathbf{x})$ and \mathbf{A}_s are block lower triangular with respect to the splitting $\mathbf{x} = (\mathbf{x}^{[0]}, \mathbf{x}^{[1]}, \mathbf{x}^{[2]})$, when we apply the construction of Theorem 2.5, injectivity of the Jacobian (see Remark 2.6) implies injectivity of $D_{\mathbf{x}}\mathbf{H}_s(\hat{\mathbf{x}}^{[0]}(s))$.

Lemma 3.6. Let the conditions of Theorem 2.5 be satisfied for the extended system \mathbf{H}_s and assume that the corresponding smoothness condition (3.1) holds. Then $\hat{\mathbf{x}}(s) = \hat{\mathbf{x}}^{[0]}(s)$ solves $H_s(x) = 0$, while $\hat{\mathbf{x}}^{[1]}(s) = \hat{\mathbf{x}}'(s)$ and $\hat{\mathbf{x}}^{[2]}(s) = \hat{\mathbf{x}}''(s)$.

Proof. This follows from the equivalence of $\mathbf{H}_s(\mathbf{x})$ and (3.4), as well as Remarks 3.3 and 3.5. \square

We now assume we have successfully applied Theorem 2.5 to \mathbf{H}_s . In particular, let $\hat{\mathbf{x}}_0 = (\hat{v}_0, \hat{\lambda}_0)$ and $\hat{\mathbf{x}}_1 = (\hat{v}_1, \hat{\lambda}_1)$ be the end points of a line segment for which we have found, through Theorem 2.5, a solution curve

$$\hat{\mathbf{x}}(s) = (\hat{v}, \hat{\lambda})(s) \in \mathcal{C}_{\hat{r}} \quad \text{for } s \in [0, 1]. \quad (3.6)$$

We also assume that the corresponding smoothness condition (3.1) holds, so that we may apply Lemma 3.6. Then we can use the following result to verify that a nondegenerate saddle-node bifurcation occurs.

Proposition 3.7. Let $1 \leq j \leq m$. Assume

$$(\hat{\lambda}_0^{[1]})_j + \hat{r} < 0, \quad (3.7a)$$

$$(\hat{\lambda}_1^{[1]})_j - \hat{r} > 0, \quad (3.7b)$$

$$\min\{(\hat{\lambda}_0^{[2]})_j, (\hat{\lambda}_1^{[2]})_j\} - \hat{r} > 0. \quad (3.7c)$$

Then the solutions curve $\hat{\mathbf{x}}(s)$ undergoes a unique nondegenerate fold bifurcation (folding to the right) with respect to λ_j in the interval $s \in [0, 1]$.

Proof. Let $\hat{\lambda}_j(s) = \hat{\lambda}_j^{[0]}(s)$. For $i = 0, 1, 2$, denote $\hat{\lambda}_s^{[i]} = (1-s)\hat{\lambda}_0^{[i]} + s\hat{\lambda}_1^{[i]}$. For $i = 0, 1, 2$, let $\hat{\lambda}_j^{(i)}(s)$ denote the i -th derivative of $\hat{\lambda}_j(s)$. It follows from Lemma 3.6 and Equation (3.6) that

$$|\hat{\lambda}_j^{(i)}(s) - (\hat{\lambda}_s^{[i]})_j| = |\hat{\lambda}_j^{[i]}(s) - (\hat{\lambda}_s^{[i]})_j| \leq \hat{r} \quad \text{for } i = 0, 1, 2. \quad (3.8)$$

It then follows from (3.7a)–(3.7b) that $\hat{\lambda}_j'(0) < 0$ while $\hat{\lambda}_j'(1) > 0$, hence by the intermediate value theorem there exists an $s_\star \in (0, 1)$ such that $\hat{\lambda}_j'(s_\star) = 0$. Furthermore, since

$$(\hat{\lambda}_s^{[2]})_j = (1-s)(\hat{\lambda}_0^{[2]})_j + s(\hat{\lambda}_1^{[2]})_j,$$

it follows from (3.8) and (3.7c) that $\hat{\lambda}_j''(s) > 0$ for all $s \in [0, 1]$. In particular, $\hat{\lambda}_j''(s_\star) > 0$ and $\hat{\lambda}_j(s) \geq \hat{\lambda}_j(s_\star)$ for all $s \in [0, 1]$, and besides $s = s_\star$ there is no other zero of $\hat{\lambda}_j'(s)$ on $[0, 1]$. \square

Alternative conditions which lead to the same result, but with the curve folding to the left, are

$$(\hat{\lambda}_0^{[1]})_j - \hat{r} > 0, \quad (3.9a)$$

$$(\hat{\lambda}_1^{[1]})_j + \hat{r} < 0, \quad (3.9b)$$

$$\max\{(\hat{\lambda}_0^{[2]})_j, (\hat{\lambda}_1^{[2]})_j\} + \hat{r} < 0. \quad (3.9c)$$

Remark 3.8. *Since the stepsize may be quite (or even very) small in practice, the first derivative $\hat{\mathbf{x}}^{[1]}(s) = (\hat{\mathbf{x}}^{[0]})'(s)$ can be of an entirely different size than $\hat{\mathbf{x}}^{[0]}(s)$, and for the second derivative this holds a fortiori. In such a situation, the variable components $\mathbf{x}^{[0]}$, $\mathbf{x}^{[1]}$ and $\mathbf{x}^{[2]}$ are not of commensurable magnitude, and a uniform norm, as in (2.5) is not appropriate, and indeed using it unaltered makes the conditions (3.7) unachievable. This obstacle is overcome by rescaling the variable components $\mathbf{x}^{[1]}$ and $\mathbf{x}^{[2]}$ appropriately, with scale parameters that are linear and quadratic in the stepsize, respectively.*

Furthermore, since inequalities (3.7a)–(3.7b) are evaluated in the endpoints only, we may apply a noncontinuation version of Theorem 2.5 to each endpoint separately (for the smaller extended system discussed in Remark 3.9), which helps in verifying (3.7a)–(3.7b).

Remark 3.9. *In a similar, but easier, fashion one may verify that no bifurcation occurs with respect to $\lambda_{j'}$ by checking that*

$$\min\left\{(\hat{\lambda}_0^{[1]})_{j'}, (\hat{\lambda}_1^{[1]})_{j'}\right\} - \hat{r} > 0 \quad \text{or} \quad \max\left\{(\hat{\lambda}_0^{[1]})_{j'}, (\hat{\lambda}_1^{[1]})_{j'}\right\} + \hat{r} < 0.$$

Naturally, since this does not involve the second derivative, if one merely wants to exclude bifurcations it suffices to apply Theorem 2.5 to the smaller extended system for $(\mathbf{x}^{[0]}, \mathbf{x}^{[1]})$.

4 Eigenvalue considerations

Traditionally, saddle-node bifurcations are identified in terms of a simple eigenvalue crossing 0. Here we discuss how our nondegenerate folds, as described in Definition 3.1 by the local parabolicity in (3.3) of the solution curve, relates to such eigenvalue considerations. We consider the case of a fold bifurcation for (1.2) with respect to $\lambda_2 = \mu$. In particular, $\lambda = (\tau, \mu) \in \mathbb{R}^2$ and $h : \mathbb{R}^n \times \mathbb{R}^2 \rightarrow \mathbb{R}^n$ is given by $\tau f(u, \mu)$, where f is the vector field in (1.1) and τ is the normalized period.

We start by describing the information on the eigenvalues of $D_x H_s(\hat{x}(s))$, and subsequently relate this to stability information for the periodic orbits of (1.1). We collect the variables v and τ in $w = (v, \tau) \in \tilde{X} = (\ell_\nu^1)^n \times \mathbb{C}$. Let

$$\tilde{H}(x) \stackrel{\text{def}}{=} \begin{bmatrix} F(x) \\ G^\mathbb{C}(x) \end{bmatrix} = 0.$$

We then write

$$D_x H_s(\hat{x}(s)) = \begin{bmatrix} D_w \tilde{H}(\hat{x}(s)) & D_\mu \tilde{H}(\hat{x}(s)) \\ q_w^\circ(s) & q_\mu^\circ(s) \end{bmatrix}, \quad (4.1)$$

where we unravel the notation for the continuation equation (2.10) through the use of $q_s^\circ = (q_w^\circ, q_\mu^\circ)(s) = (q_v^\circ, q_\tau^\circ, q_\mu^\circ)(s)$. We infer from Remark 2.6 that $D_x H_s(\hat{x}(s))$ is invertible as a map from X to $X_1 = (\ell_{\nu,1}^1)^n \times \mathbb{C}^m$, where

$$\ell_{\nu,1}^1 \stackrel{\text{def}}{=} \{\tilde{v} \in \ell_\nu^1 : K\tilde{v} \in \ell_\nu^1\},$$

which is a Banach space when equipped with the norm $\|\tilde{v}\|_{\nu,1} = \sum_{k \in \mathbb{Z}} |\tilde{v}_k| \nu^{|k|} (|k| + 1)$.

Our central object of interest is

$$\mathcal{Q}_s \stackrel{\text{def}}{=} D_w \tilde{H}(\hat{x}(s)),$$

which is conjugation invariant, i.e., $\mathcal{Q}_s w^* = (\mathcal{Q}_s w)^*$, since \tilde{H} is and $\hat{x}(s) \in \mathcal{S}$. Furthermore, \mathcal{Q}_s is a bounded operator from \tilde{X} to $\tilde{X}_1 \stackrel{\text{def}}{=} (\ell_{\nu,1}^1)^n \times \mathbb{C}$, but it may also be interpreted as an unbounded operator on \tilde{X} . Finally, \mathcal{Q}_s is Fredholm of index 0.

We note that, by differentiating the identity $\tilde{H}(\hat{x}(s)) = 0$ with respect to s , we have

$$\mathcal{Q}_s \dot{w}'(s) + D_\mu \tilde{H}(\hat{x}(s)) \dot{\mu}'(s) = 0. \quad (4.2)$$

Hence at $s = s_*$, where $\dot{\mu}'(s_*) = 0$, we have that \mathcal{Q}_{s_*} , and thus $D_w \tilde{H}(\hat{x}(s_*))$, has $\dot{w}'(s_*)$ as an eigenvector associated to the zero eigenvalue. Indeed $\dot{w}'(s_*)$ is not trivial in view of smoothness of the solution curve (Inequality (3.1)).

The next remark guarantees that \mathcal{Q}_s does not have a zero eigenvalue for $s \neq s_*$.

Remark 4.1. *If \mathcal{Q}_s has an eigenvector w_0 associated to the zero eigenvalue for some $s \in [0, 1]$, then it follows from invertibility of $D_x H_s(\hat{x}(s))$ that $\langle q_w^\circ(s), w_0 \rangle \neq 0$. In turn it follows that $W_0 \stackrel{\text{def}}{=} (c_0 w_0, 0)$ with*

$$c_0 \stackrel{\text{def}}{=} -\frac{D_s G_s^\circ(\hat{x}(s))}{\langle q_w^\circ(s), w_0 \rangle},$$

solves $D_x H_s(\hat{x}(s))W_0 = -D_s H_s(\hat{x}(s))$. Hence, by invertibility of $D_x H_s(\hat{x}(s))$, we find that $\hat{x}'(s) = (c_0 w_0, 0)$, because we have the identity

$$D_x H_s(\hat{x}(s))\hat{x}'(s) + D_s H_s(\hat{x}(s)) = 0 \quad \text{for all } s \in [0, 1].$$

In particular, this implies that $\dot{\mu}'(s) = 0$, so that we conclude from the uniqueness statement in Proposition 3.7 that \mathcal{Q}_s has eigenvalue zero at $s = s_$ only.*

Next we argue that the geometric multiplicity of the zero eigenvalue of \mathcal{Q}_{s_*} is 1. Namely, if the 0-eigenspace of \mathcal{Q}_{s_*} is two (or higher) dimensional, then it is straightforward to construct a nontrivial element in the kernel of $D_x H_s(\hat{x}(s))$, which contradicts its injectivity, which was established in Remark 2.6. It will take a bit more work (see below) to analyze the *algebraic* multiplicity of the zero eigenvalue, which may be higher than 1.

We introduce the dual space $\tilde{X}' = (\ell_{\nu-1}^\infty)^n \times \mathbb{C}$, where $\ell_{\nu-1}^\infty \stackrel{\text{def}}{=} \{\tilde{v} \in \mathbb{C}^{\mathbb{Z}} : \sup_{k \in \mathbb{Z}} |\tilde{v}_k| \nu^{-|k|} < \infty\}$, and let $\tilde{w}_* \in \tilde{X}'$ be an eigenvector of the transpose \mathcal{Q}'_{s_*} associated to the zero eigenvalue. Here the transpose has the usual definition: $\langle \mathcal{Q}'_{s_*} \tilde{w}, w \rangle = \langle \tilde{w}, \mathcal{Q}_{s_*} w \rangle$ for all $w \in \tilde{X}$, $\tilde{w} \in \tilde{X}'$, where the dual pairing uses the slightly abused notation, cf (2.6),

$$\langle \tilde{w}, w \rangle = \sum_{i=1}^n \sum_{k \in \mathbb{Z}} (\tilde{v}_i)_k (v_i)_k + \check{\tau} \tau.$$

Since we can restrict \mathcal{Q}_{s_*} to the conjugate symmetric set $\{w \in \tilde{X} : w^* = w\}$, and the eigenvector $\dot{w}'(s_*)$ lies in this set, we may also assume that $\tilde{w}_*^* = \tilde{w}_*$. Then the range of \mathcal{Q}_{s_*} can be characterized as

$$\text{Range } \mathcal{Q}_{s_*} = \{w \in \tilde{X}_1 : \langle \tilde{w}_*, w \rangle = 0\}. \quad (4.3)$$

We now use a standard trick to obtain information about eigenvalues. Let $0 \neq \tilde{w}_*$ be such that $\mathcal{Q}'_{s_*} \tilde{w}_* = 0$. Invertibility of $D_x H_s(\hat{x}(s))$ implies that its transpose is invertible as a linear map from X'_1 to X' . Hence we see from (4.1) that

$$\langle \tilde{w}_*, D_\mu \tilde{H}(\hat{x}(s_*)) \rangle \neq 0. \quad (4.4)$$

The second derivative $\hat{x}''(s) = (\dot{w}''(s), \dot{\mu}''(s))$ satisfies

$$\begin{aligned} D_w \tilde{H}(\hat{x}(s))\dot{w}''(s) + D_\mu \tilde{H}(\hat{x}(s))\dot{\mu}''(s) = \\ - D_{w,w}^2 \tilde{H}(\hat{x}(s))[\dot{w}'(s), \dot{w}'(s)] - 2D_{w,\mu}^2 \tilde{H}(\hat{x}(s))[\dot{w}'(s), \dot{\mu}'(s)] - D_{\mu,\mu}^2 \tilde{H}(\hat{x}(s))[\dot{\mu}'(s), \dot{\mu}'(s)]. \end{aligned}$$

When we evaluate this at $s = s_*$ and apply \tilde{w}_* to the result, we obtain

$$\langle \tilde{w}_*, D_\mu \tilde{H}(\hat{x}(s_*)) \rangle \dot{\mu}''(s_*) = -\langle \tilde{w}_*, D_{w,w}^2 \tilde{H}(\hat{x}(s_*))[\dot{w}'(s_*), \dot{w}'(s_*)] \rangle. \quad (4.5)$$

Since $\mu''(s_\star) \neq 0$ by nondegeneracy of the fold (see (3.3) and Proposition 3.7), we conclude from (4.4) and (4.5) that

$$\langle \check{w}_\star, D_{w,w}^2 \tilde{H}(\check{x}(s_\star))[\check{w}'(s_\star), \check{w}'(s_\star)] \rangle \neq 0. \quad (4.6)$$

We note that all of the elements \check{w}_\star , $D_\mu \tilde{H}(\check{x}(s_\star))$ and $D_{w,w}^2 H_s(\check{x}(s_\star))[\check{w}'(s_\star), \check{w}'(s_\star)]$ are conjugate symmetric, which is consistent with $\check{\mu}''(s_\star)$ being real.

We are now ready to analyze the situation associated to higher algebraic multiplicity of the zero eigenvalue. The eigenvalue problem for \mathcal{Q}_s is

$$\mathcal{R}_\alpha(w, s) \stackrel{\text{def}}{=} \left[\begin{array}{c} \mathcal{Q}_s w - \alpha w \\ \langle q_w^\circ(s_\star), w \rangle - \langle q_w^\circ(s_\star), \check{w}'(s_\star) \rangle \end{array} \right] = 0,$$

which has a zero $\mathcal{R}_0(\check{w}'(s_\star), s_\star) = 0$. The derivative at this zero is

$$D\mathcal{R}_0 = \left[\begin{array}{cc} \mathcal{Q}_{s_\star} & D_{w,w}^2 \tilde{H}(\check{x}(s_\star))[\check{w}'(s_\star), \check{w}'(s_\star)] \\ q_w^\circ(s_\star) & 0 \end{array} \right].$$

Since $D_x H_{s_\star}(\check{x}(s_\star))$ is invertible we infer that, see (4.1), the range of

$$\left[\begin{array}{c} \mathcal{Q}_{s_\star} \\ q_w^\circ(s_\star) \end{array} \right]$$

has co-dimension 1 in X_1 . It then follows from (4.3) and (4.6) that $D\mathcal{R}_0$ is invertible. Hence we conclude from the implicit function theorem that $\mathcal{R}_\alpha(w, s) = 0$ has a locally unique smooth branch of solutions $\mathcal{R}_\alpha(\bar{w}(\alpha), \bar{s}(\alpha)) = 0$.

The local dependence of \bar{s} on α is governed by the algebraic multiplicity of the zero eigenvalue as follows. By differentiating $D_w \tilde{H}(\check{x}(\bar{s}(\alpha)))\bar{w}(\alpha) - \alpha\bar{w}(\alpha) = 0$ with respect to α we obtain

$$\begin{aligned} D_{w,w}^2 \tilde{H}(\check{x}(\bar{s}(\alpha)))[\check{w}'(\bar{s}(\alpha)), \bar{w}(\alpha)]\bar{s}'(\alpha) + D_{\mu,w}^2 \tilde{H}(\check{x}(\bar{s}(\alpha)))[\check{\mu}'(\bar{s}(\alpha)), \bar{w}(\alpha)]\bar{s}'(\alpha) \\ + D_w \tilde{H}(\check{x}(\bar{s}(\alpha)))\bar{w}'(\alpha) - \alpha\bar{w}'(\alpha) - \bar{w}(\alpha) = 0. \end{aligned} \quad (4.7)$$

Substituting $\alpha = 0$ we obtain (recalling that $\mathcal{Q}_{s_\star} = D_w \tilde{H}(\check{x}(s_\star))$)

$$D_{w,w}^2 \tilde{H}(\check{x}(s_\star))[\check{w}'(s_\star), \check{w}'(s_\star)]\bar{s}'(0) + \mathcal{Q}_{s_\star} \bar{w}'(0) = \bar{w}(0), \quad (4.8)$$

and applying \check{w}_\star to this result leads to

$$\langle \check{w}_\star, D_{w,w}^2 \tilde{H}(\check{x}(s_\star))[\check{w}'(s_\star), \check{w}'(s_\star)] \rangle \bar{s}'(0) = \langle \check{w}_\star, \check{w}'(s_\star) \rangle. \quad (4.9)$$

We see from (4.6) that $\bar{s}'(0) \neq 0$ if and only if $\langle \check{w}_\star, \check{w}'(s_\star) \rangle \neq 0$. In view of (4.3) the latter is equivalent to $\check{w}'(s_\star)$ not being in the range of \mathcal{Q}_{s_\star} , i.e., the algebraic multiplicity of the zero eigenvalue being 1. The contrapositive is that $\bar{s}'(0)$ vanishes if the algebraic multiplicity is larger than 1. We consider each case below.

In the former (algebraic multiplicity 1) case we see from (4.9), combined with conjugate symmetry of \check{w}_\star , that $D_{w,w}^2 \tilde{H}(\check{x}(s_\star))[\check{w}'(s_\star), \check{w}'(s_\star)]$ and $\check{w}'(s_\star)$, that $\bar{s}'(0) \in \mathbb{R} \setminus \{0\}$. By inverting the relation, we find that $\alpha = (\bar{s}'(0))^{-1}(s - s_\star) + O((s - s_\star)^2)$, hence the eigenvalue crosses zero with nonzero speed as we go through the fold and we have a classical saddle-node bifurcation.

In the latter (algebraic multiplicity larger than 1) case we differentiate (4.7) again, and substitute $\alpha = 0$. Using the information that $\bar{s}'(0) = 0$ and

$$D_w \tilde{H}(\check{x}(s_\star))\bar{w}'(0) = \bar{w}(0), \quad (4.10)$$

which follows from (4.8), we obtain

$$D_{w,w}^2 \tilde{H}(\hat{x}(s_\star))[\hat{w}'(s_\star), \hat{w}'(s_\star)]\bar{s}''(0) + \mathcal{Q}_{s_\star} \bar{w}''(0) = 2\bar{w}'(0).$$

Once again applying \check{w}_\star to this, we find

$$\langle \check{w}_\star, D_{w,w}^2 \tilde{H}(\hat{x}(s_\star))[\hat{w}'(s_\star), \hat{w}'(s_\star)]\bar{s}''(0) \rangle = 2\langle \check{w}_\star, \bar{w}'(0) \rangle.$$

There are two possible scenarios. Either $\bar{s}''(0) \neq 0$ and $\bar{w}'(0)$ is not in range of \mathcal{Q}_{s_\star} and thus, in view of (4.10), the algebraic multiplicity of the zero eigenvalue is 2. Or $\bar{s}''(0) = 0$ and $\mathcal{Q}_{s_\star} \bar{w}''(0) = 2\bar{w}'(0)$ and the algebraic multiplicity of the zero eigenvalue is larger than 2.

We can now repeat the above arguments inductively. We conclude that $s = s_\star + C\alpha^N + O(\alpha^{N+1})$ for some $C \in \mathbb{R} \setminus \{0\}$, where N is the algebraic multiplicity of the zero eigenvalue of $\mathcal{Q}_{s_\star} = D_w \tilde{H}(\hat{x}(s_\star))$ at the fold (which always has geometric multiplicity 1). Inverting the relation, we see that $\alpha = C^{1/N}(s - s_\star)^{1/N} + O((s - s_\star)^{(N+1)/N})$, which gives detailed information on the dynamics of the N eigenvalues of $\mathcal{Q}_s = D_w \tilde{H}(\hat{x}(s))$ that coalesce at 0 when we move through the fold. In particular, the number of negative eigenvalues changes by 1 (not counting complex conjugate pairs).

Before we discuss the implications of this information for the eigenvalue problem of $D_v F(\hat{x}(s))$, we exclude some marginal behaviour. More precisely, in the next two remarks, we exclude two possible “trivialities” of the fold.

Remark 4.2. *First, the solution at the fold cannot be an equilibrium solution. By contradiction, assume that $\hat{v}_k(s_\star) = 0$ for all $k \neq 0$, and $f(\hat{v}_0(s_\star), \hat{\mu}(s_\star)) = 0$. We write*

$$D_w \tilde{H}(\hat{x}(s_\star)) = \begin{bmatrix} D_v F(\hat{x}(s_\star)) & D_\tau F(\hat{x}(s_\star)) \\ q_v^\mathbb{C} & 0 \end{bmatrix}. \quad (4.11)$$

Since the kernel of $D_w \tilde{H}(\hat{x}(s_\star))$ is one dimensional, and $D_\tau F(\hat{x}(s_\star)) = f(\hat{v}_0(s_\star), \hat{\mu}(s_\star))$ vanishes, we conclude that that $(v, \tau) = (0, 1)$ spans the kernel. By differentiating the identity $\tilde{H}(\hat{x}(s)) = 0$ with respect to s , evaluating at $s = s_\star$ and using that $\hat{\mu}'(s_\star) = 0$, we then conclude that $\hat{v}'(s_\star) = 0$ and $\hat{\tau}'(s_\star) \neq 0$. In turn this implies that

$$D_{w,w}^2 \tilde{H}(\hat{x}(s_\star))[\hat{w}'(s_\star), \hat{w}'(s_\star)] = D_{\tau,\tau}^2 \tilde{H}(\hat{x}(s_\star))[\hat{\tau}'(s_\star), \hat{\tau}'(s_\star)],$$

which vanishes since \tilde{H} is linear in τ . This contradicts (4.6).

Remark 4.3. *The second scenario that we would like to exclude is that the fold inadvertently occurs due to a shift in time. In particular, we want to confirm that*

$$\langle q_v^\mathbb{C}, iK\hat{v}(s_\star) \rangle \neq 0.$$

This is achieved through a computational check, cf. the smoothness condition (3.1):

$$\hat{r} \langle q^\mathbb{C}, b \rangle \neq \langle q^\mathbb{C}, iK[(1-s)\hat{x}_0 + s\hat{x}_1] \rangle \quad \text{for any } s \in [0, 1] \text{ and } b \in B_1(0),$$

which in practice is satisfied since $\overline{iK\hat{x}_0} \approx q^\mathbb{C} \approx \overline{iK\hat{x}_1}$ and $\hat{r} \ll 1$.

We now relate eigenvalues of \mathcal{Q}_s to eigenvalues of $D_v F(\hat{x}(s))$, which in turn correspond to characteristic multipliers of the periodic solution

$$\hat{u}(t) = \sum_{k \in \mathbb{Z}} \hat{v}_k e^{ikt}.$$

Namely, an eigenvalue-eigenvector pair $(\tilde{\alpha}, \tilde{a})$ of $D_v F(\hat{x}(s))$ solves

$$iK\tilde{a} - \hat{\tau}(s)D_v \hat{f}(\hat{v}(s), \hat{\mu}(s))\tilde{a} = \tilde{\alpha}\tilde{a}.$$

Hence $a(t) = \sum_{k \in \mathbb{Z}} \tilde{a}_k e^{ikt}$ is a 2π -periodic solution of the linearized problem

$$\dot{a}(t) - \hat{\tau}(s)D_u f(\hat{u}(t; s), \hat{\mu}(s))a(t) = \tilde{\alpha}a(t),$$

and $e^{2\pi\tilde{\alpha}}$ is thus a characteristic multiplier of the system. In particular, the eigenvalues of $D_v F(\hat{x}(s))$ contain the information about linearized stability of the periodic orbit \hat{u} . We now return to the relation between the eigenvalues of \mathcal{Q}_s and the eigenvalues of $D_v F(\hat{x}(s))$.

Let $\tilde{w} = (\tilde{v}, \tilde{\tau})$ be an eigenvector with eigenvalue α of \mathcal{Q}_s . For generalized eigenvectors a similar analysis goes through; we leave the details to the reader. Since $D_v F(\hat{x}(s))$ has a zero eigenvector $V_0 \stackrel{\text{def}}{=} i\tau_0^{-1}K\hat{v}(s)$, with $\tau_0 \stackrel{\text{def}}{=} \hat{\tau}(s)$, and $D_\tau F(\hat{x}(s)) = -\hat{f}(\hat{x}(s)) = -iK\tau_0^{-1}\hat{x}(s) = -V_0$, we infer that

$$\mathcal{Q}_s \begin{bmatrix} \tilde{v} \\ \tilde{\tau} \end{bmatrix} = \begin{bmatrix} D_v F(\hat{x}(s)) & -V_0 \\ q_v^{\mathbb{C}} & 0 \end{bmatrix} \begin{bmatrix} \tilde{v} \\ \tilde{\tau} \end{bmatrix} = \alpha \begin{bmatrix} \tilde{v} \\ \tilde{\tau} \end{bmatrix}. \quad (4.12)$$

In view of Remark 4.3 we have that $\langle q_v^{\mathbb{C}}, V_0 \rangle \neq 0$ for s near s_* .

We now consider three cases: $\alpha = 0$, $\alpha^2 = -\langle q_v^{\mathbb{C}}, V_0 \rangle$, and all other α .

If $\alpha = 0$ then it follows immediately from (4.12) that $D_v F(\hat{x}(s))\tilde{v} = \tilde{\tau}V_0$, hence \tilde{v} is either an eigenvector or a generalized eigenvector for eigenvalue zero of $D_v F(\hat{x}(s))$. Furthermore, \tilde{v} is not a multiple of V_0 since $\langle q_v^{\mathbb{C}}, \tilde{v} \rangle = 0$.

If $\alpha \neq 0$ and $\alpha^2 \neq -\langle q_v^{\mathbb{C}}, V_0 \rangle$, then we set $\tilde{V} = \tilde{v} + \frac{\tilde{\tau}}{\alpha}V_0$ and we conclude from (4.12) that $D_v F(\hat{x}(s))\tilde{V} = \alpha\tilde{V}$. Additionally we find $\langle q_v^{\mathbb{C}}, \tilde{v} \rangle = \alpha\tilde{\tau}$, hence if $\tilde{\tau} \neq 0$ then $\langle q_v^{\mathbb{C}}, \tilde{V} \rangle = \frac{\tilde{\tau}}{\alpha}(\alpha^2 + \langle q_v^{\mathbb{C}}, V_0 \rangle) \neq 0$. We infer that \tilde{V} is an eigenvector of $D_v F(\hat{x}(s))$ with eigenvalue α . If $\tilde{\tau} = 0$ then $\tilde{V} = \tilde{v} \neq 0$ and we reach the same conclusion.

If $\alpha^2 = -\langle q_v^{\mathbb{C}}, V_0 \rangle$, then $(\tilde{v}, \tilde{\tau}) = (V_0, -\alpha)$ solves (4.12). There is no relation to eigenvalues of $D_v F(\hat{x}(s))$.

Finally, we note that since $\langle q_v^{\mathbb{C}}, V_0 \rangle \neq 0$ at $s = s_*$, the eigenvalues $\alpha \approx C^{1/N}(s - s_*)^{1/N}$ emanating from a fold bifurcation all correspond to eigenvalues of $D_v F(\hat{x}(s_*))$ and hence to characteristic multipliers of the periodic orbit $\hat{u}(t)$.

5 Hopf bifurcation

A Hopf bifurcation is characterized by the junction of a family of equilibria and a family of periodic orbits. Let $\check{y}(\mu)$ denote a smooth family of equilibria: $f(\check{y}(\mu), \mu) = 0$ for $\mu \in [\mu_0, \mu_1]$. Let $\{\hat{x}(s)\}_{s \in [0, 1]}$ be a solution curve of periodic orbits of (1.1), using the notation introduced in Section 2. We write $\hat{x}(s) = (\hat{v}(s), \hat{\tau}(s), \hat{\mu}(s))$.

In a Hopf bifurcation we have $\hat{v}(s_*) = \check{y}(\mu(s_*))$, which is to be interpreted as meaning that the Fourier coefficients $\hat{v}(s_*)$ correspond to the *stationary* state $\check{y}(\mu(s_*))$.

Definition 5.1. We say that there is a *nondegenerate Hopf bifurcation* (with respect to μ) at $\mu_* \in (\mu_1, \mu_2)$ if there is an $s_* \in (0, 1)$ such that

$$\hat{\mu}(s_*) = \mu_* \quad \text{and} \quad \hat{v}(s_*) = \check{y}(\mu_*),$$

while $\hat{v}(s)$ is not a stationary solution for any $s \neq s_*$, and

$$\hat{\mu}'(s_*) = 0, \quad \hat{\mu}''(s_*) \neq 0. \quad (5.1)$$

In this section we explain how to establish such nondegenerate Hopf bifurcations using a blowup (or desingularization) technique. Note that we do not impose any eigenvalue restrictions in the description (3.3) of a nondegenerate Hopf bifurcation.

Remark 5.2. *Hopf bifurcations with respect to the normalized period τ also fit into our framework. Although they are not Hopf bifurcations in the traditional sense, these do appear naturally when studying Hamiltonian problems, or stationary states in partial differential equations with periodic boundary conditions when varying the size of the domain. In Section 7.4 we present an example.*

As already explained in the introduction, we rescale time and put ourselves in the context of (1.2). In effect, we set $\lambda = (\tau, \mu)$ and replace f by $\tilde{f} = \tau f$. To resolve a branch of periodic orbits all the way into the Hopf bifurcation, we introduce the rescaling $u(t) = y + a\bar{u}(t)$, with $a \in \mathbb{R}$, and $y = y(\mu) \in \mathbb{R}^n$ solving

$$f(y, \mu) = 0.$$

The ODE for \bar{u} becomes

$$\dot{\bar{u}} = \bar{f}(\bar{u}, \bar{\lambda}) \stackrel{\text{def}}{=} \begin{cases} \frac{\tilde{f}(y+a\bar{u}, \lambda) - \tilde{f}(y, \lambda)}{a} & \text{if } a \neq 0, \\ D_u \tilde{f}(y, \lambda) \bar{u} & \text{if } a = 0, \end{cases} \quad (5.2)$$

where $\bar{\lambda} = (\tau, a, y, \mu)$. We note that \bar{f} is again polynomial in \bar{u} (as well as in a and y). Setting $\bar{g}(\bar{\lambda}) = f(y, \mu) \in \mathbb{R}^n$ the system

$$\begin{cases} \dot{\bar{u}} = \bar{f}(\bar{u}, \bar{\lambda}), \\ \bar{g}(\bar{\lambda}) = 0, \\ \bar{u}(t) \text{ is } 2\pi\text{-periodic,} \end{cases} \quad (5.3)$$

is again of the form (2.1). What remains is to introduce appropriate phase and continuation equations, as well as an ‘‘amplitude’’ equation which lifts the invariance under the continuous rescaling $a \rightarrow \theta^{-1}a$ and $\bar{u}(t) \rightarrow \theta\bar{u}(t)$ for $\theta \in \mathbb{R}$.

We collect all the variables in $x = (v, \bar{\lambda})$, where v denotes the Fourier coefficients of \bar{u} . As in Section 2 we assume we have two points $\hat{x}_0 = (\hat{v}_0, \hat{\lambda}_0) \in \mathcal{S}_K$ and $\hat{x}_1 = (\hat{v}_1, \hat{\lambda}_1) \in \mathcal{S}_K$ which each represent an approximate solution of the Fourier equivalent of (5.3). While it is now hidden in the notation that we are solving (5.3) rather than (1.2), we use the same phase condition as in Section 2: $G^{\mathbb{C}}(x) = \langle q^{\mathbb{C}}, x \rangle = 0$, where $q^{\mathbb{C}} = (q_v^{\mathbb{C}}, 0) \in X_K$ is given by (2.8). For the amplitude equation $G^{\oplus}(x)$ we use

$$G^{\oplus}(x) \stackrel{\text{def}}{=} \langle q^{\oplus}, x \rangle - 1 = 0, \quad (5.4)$$

where $q^{\oplus} = (q_v^{\oplus}, 0) \in \mathcal{S}_K$, with

$$(q_v^{\oplus})_i = \overline{K^2(\hat{v}_{\frac{1}{2}})_i} \quad \text{for } |k| \leq K, 1 \leq i \leq n. \quad (5.5)$$

We will slightly abuse the notation for the bilinear form to write $\langle q^{\oplus}, x \rangle = \langle q_v^{\oplus}, v \rangle$, and by $[q_v^{\oplus}]_k \in \mathbb{C}^n$ we will denote the k -th Fourier component of q_v^{\oplus} . With the choice (5.5) the corresponding Equation (5.4) represents a linear approximation of

$$\frac{1}{2\pi} \int_0^{2\pi} \sum_{i=1}^n |\dot{\bar{u}}_i(t)|^2 dt = 1.$$

Finally, the continuation equation $G_s^{\odot}(x) = 0$ is chosen as in Section 2, see (2.10), where the ‘‘predictors’’ \hat{x}_s are now of the tangent direction of the solution curve for the problem including both the phase and the amplitude condition.

Denoting by \bar{F} the Fourier transform of the renormalized vector field (5.2), the full set of equations becomes

$$\bar{H}_s(x) = \begin{bmatrix} \bar{F}(x) \\ \bar{G}_s(x) \end{bmatrix} \quad \text{with} \quad \bar{G}_s(x) = \begin{bmatrix} G^{\mathbb{C}}(x) \\ G^{\oplus}(x) \\ \bar{g}(\bar{\lambda}) \\ G_s^{\ominus}(x) \end{bmatrix}.$$

For $\bar{H}_s(x) = 0$ we then carry out the extension construction of Section 3, leading to the problem $\bar{\mathbf{H}}_s(x) = 0$. To the latter we apply the technique from Theorem 2.5 to obtain a parametrized solution curve $\hat{x}(s) = (\hat{v}, \hat{\lambda})(s)$. The first ‘‘block’’ $\hat{x}^{[0]} = (\hat{v}^{[0]}, \hat{\lambda}^{[0]})$ corresponds to $\hat{\lambda}^{[0]}(s) = \hat{\lambda}(s) = (\hat{\tau}(s), \hat{a}(s), \hat{y}(s), \hat{\mu}(s))$ and the Fourier coefficients of $\hat{u}(t; s)$. The second block $\hat{x}^{[1]}$ contains the first derivatives $(\hat{\tau}'(s), \hat{a}'(s), \hat{y}'(s), \hat{\mu}'(s))$ and the Fourier coefficients of $\partial_s \hat{u}(t; s)$, while $\hat{x}^{[2]}$ contains their second derivatives.

Before we can properly formulate the result, we need to analyze the problem at $a = 0$. In particular, we aim to establish that $\hat{a}(s_0) = 0$ implies $\hat{\mu}'(s_0) = 0$. Hence suppose $\hat{a}(s_0) = 0$ for some $s_0 \in (0, 1)$. We denote the Jacobian of the equilibrium problem by

$$A_0 \stackrel{\text{def}}{=} D_u f(\hat{y}(s_0), \hat{\mu}(s_0)).$$

Then, since \bar{f} is linear in \bar{u} at $a = 0$,

$$(\bar{F}(\hat{x}(s_0)))_k = (ikI_n - \hat{\tau}(s_0)A_0)\hat{v}_k(s_0) = 0, \quad \text{for all } k \in \mathbb{Z}, \quad (5.6)$$

with $\hat{v}_k(s_0) \in \mathbb{C}^n$ and I_n the identity matrix on \mathbb{C}^n , i.e., the ODE is diagonalized (in k) in Fourier space. Since $\langle q_v^{\oplus}, \hat{v}(s_0) \rangle = 1$, and $[q_v^{\oplus}]_0 = 0$, there must be at least one $k_0 \in \mathbb{Z} \setminus \{0\}$ such that

$$M_{k_0} \stackrel{\text{def}}{=} ik_0 I_n - \hat{\tau}(s_0)A_0$$

is a non-invertible matrix. We note that this implies that $\hat{\tau}(s_0) \neq 0$. By conjugation symmetry M_{-k_0} is then non-invertible as well ($A_0 = A_0^*$ and $\hat{\tau}(s_0) \in \mathbb{R}$).

Furthermore, collecting the variables $z = (v, \tau, a, y)$ and the equations

$$\hat{H}(z, \mu) \stackrel{\text{def}}{=} \begin{bmatrix} \bar{F}(z, \mu) \\ G^{\mathbb{C}}(z) \\ G^{\oplus}(z) \\ f(y, \mu) \end{bmatrix} = 0,$$

its Jacobian can be decomposed as

$$\mathcal{P} \stackrel{\text{def}}{=} D_z \hat{H}(\hat{x}(s_0)) = \begin{bmatrix} D_v \bar{F}(\hat{x}(s_0)) & D_\tau \bar{F}(\hat{x}(s_0)) & D_a \bar{F}(\hat{x}(s_0)) & D_y \bar{F}(\hat{x}(s_0)) \\ q^{\mathbb{C}} & 0 & 0 & 0 \\ q^{\oplus} & 0 & 0 & 0 \\ 0 & 0 & 0 & A_0 \end{bmatrix}. \quad (5.7)$$

Here, again by linearity of \bar{f} at $a = a(s_0) = 0$,

$$(D_v \bar{F}(\hat{x}(s_0))v)_k = (\bar{F}(\hat{x}(s_0)))_k = (ikI_n - \hat{\tau}(s_0)A_0)v_k,$$

which is similar to (5.6) because of linearity, and

$$(D_\tau \bar{F}(\hat{x}(s_0)))_k = A_0 \hat{v}_k(s_0),$$

and

$$D_a \bar{F}(\hat{x}(s_0)) = \frac{1}{2} D_{u,u}^2 \tilde{f}(\hat{y}(s_0), \hat{\mu}(s_0))[\hat{v}(s_0), \hat{v}(s_0)], \quad (5.8)$$

which is to be interpreted in terms of convolution products, and

$$(D_y \bar{F}(\dot{x}(s_0)))_k = D_{u,u}^2 \tilde{f}(\dot{y}(s_0), \dot{\mu}(s_0)) \dot{v}_k(s_0),$$

which is to be interpreted as an $n \times n$ matrix for each $k \in \mathbb{Z}$.

Since

$$D_x H_{s_0}(\dot{x}(s_0)) = \begin{bmatrix} \mathcal{P} & D_\mu \hat{H}(\dot{x}(s_0)) \\ q_z^\ominus(s_0) & q_\mu^\ominus(s_0) \end{bmatrix} \quad (5.9)$$

is invertible, as the solution curve was obtained through Theorem 2.5, the kernel of the operator \mathcal{P} can be at most 1 dimensional. In turn this implies that the kernel of $D_v \bar{F}(\dot{x}(s_0))$ is at most 3 dimensional. Indeed this follows from the expression (5.7) for \mathcal{P} , and in particular the 0 in the lower left corner, which implies that, apart from $D_v \bar{F}(\dot{x}(s_0))$, there are only two nonzero rows in the left (block) column.

In view of $M_{\pm k_0}$ being non-invertible, the dimension of the kernel of $D_v \bar{F}(\dot{x}(s_0))$ is at least 2-dimensional. If there would be a $0 \neq k_1 \neq \pm k_0$ such that M_{k_1} is non-invertible, then M_{-k_1} would be non-invertible as well, implying that the kernel of $D_v \bar{F}(\dot{x}(s_0))$ is at least 4 dimensional, a contradiction. Hence M_k is invertible for all $k \notin \{0, \pm k_0\}$. The next remark explains why we may assume $M_0 = -\dot{\tau}(s_0) D_u f(\dot{y}(s_0), \dot{\mu}(s_0))$ to be invertible.

Remark 5.3. *Suppose M_0 is not invertible and that $\tilde{v}_0 \neq 0$ is in the kernel of M_0 . Since $\dot{\tau}(s_0) \neq 0$, the vector \tilde{v}_0 is in the kernel of A_0 , hence $(0, 0, 0, v_0)$ is in the kernel of \mathcal{P} . Furthermore, since $[q_v^\oplus]_0 = 0$ and $[q_v^\ominus]_0 = 0$, it follows that $(\tilde{V}_0, 0, 0, 0)$ is in the kernel of \mathcal{P} , where $(\tilde{V}_0)_k = 0$ for $k \neq 0$ and $(\tilde{V}_0)_0 = \tilde{v}_0$, so that \tilde{V}_0 is essentially just \tilde{v}_0 interpreted as an element of $(\ell_\nu^1)^n$. We infer that the kernel of \mathcal{P} is at least two dimensional, a contradiction. We conclude that M_0 and $A_0 = D_u f(\dot{y}(s_0), \dot{\mu}(s_0))$ are invertible matrices. It then follows from the implicit function theorem that $\dot{y}(s_0)$ is part of a smooth one parameter family of equilibria $\check{y}(\mu)$ of (1.1) with $\check{y}(\dot{\mu}(s_0)) = \dot{y}(s_0)$.*

Since M_k is invertible for $k \neq \pm k_0$, while M_{k_0} and M_{-k_0} have one-dimensional kernels (related by conjugation), it follows from (5.6) that $\dot{v}_k(s_0) = 0$ for $k \neq \pm k_0$, whereas $\dot{v}_{\pm k_0}(s_0) \neq 0$ in view of $\langle q_v^\oplus, \dot{v}(s_0) \rangle = 1$. For definiteness we will from now on, without loss of generality, assume that $k_0 = 1$. This corresponds to the linearized problem at the equilibrium $\dot{y}(s_0)$ having purely imaginary eigenvalues $\pm i \dot{\tau}(s_0)^{-1}$. Note that if $k_0 > 1$ then we may simply replace τ by τ/k_0 (and thus reduce to the minimal period). By the arguments above, the kernel of M_1 and M_{-1} is one-dimensional.

In the following we will construct an element in the kernel of \mathcal{P} . This implies, using again the arguments in Remark 4.1, that $\dot{\mu}'(s_0) = 0$. We define the 2×2 matrix

$$C \stackrel{\text{def}}{=} \begin{bmatrix} \langle [q_v^\ominus]_{-1}, \dot{v}_{-1}(s_0) \rangle & \langle [q_v^\ominus]_1, \dot{v}_1(s_0) \rangle \\ \langle [q_v^\oplus]_{-1}, \dot{v}_{-1}(s_0) \rangle & \langle [q_v^\oplus]_1, \dot{v}_1(s_0) \rangle \end{bmatrix}. \quad (5.10)$$

There are two cases to consider: C is invertible or not. We start with the latter case.

If C is non-invertible, say $0 \neq [c_-, c_+]^T$ is in its kernel, then it is easily seen that $(\tilde{v}, 0, 0, 0)$ is in the kernel of \mathcal{P} , where $\tilde{v}_k = 0$ for $k \neq \pm 1$, and $\tilde{v}_{\pm 1} = c_\pm \dot{v}_{\pm 1}(s_0)$. Hence by the arguments in Remark 4.1 $\dot{x}'(s_0)$ is a multiple of $(\tilde{v}, 0, 0, 0)$, and $\dot{\mu}'(s_0) = 0$. As a side remark, this direction can be interpreted as a combination of time-shift and rescaling a . If desired, this scenario can easily be avoided by choosing q^\ominus and q^\oplus appropriately or, alternatively, by checking that $\dot{a}'(s_0) \neq 0$, cf. Remark 5.3.

If C is invertible, then we construct an element of the form $(\tilde{v}, 0, 1, 0)$ in the kernel of \mathcal{P} . This implies, using again the arguments in Remark 4.1, that $\dot{x}'(s_0)$ is a multiple of $(\tilde{v}_0, 1, 0, 0)$ and $\dot{\mu}'(s_0) = 0$, in particular. Since M_k is invertible for $k \neq \pm 1$, and M_1 and M_{-1} have one-dimensional kernels (related by conjugation), it follows from (5.6) that $\dot{v}_k(s_0) = 0$ for $k \neq \pm 1$ and $\dot{v}_{\pm 1}(s_0) \neq 0$. We infer from (5.8) and the properties of the convolution product that $D_a \bar{F}_k(\dot{x}(s_0))$ vanishes for all $k \notin \{-2, 0, 2\}$. We set

$$\tilde{v}_k = -M_k^{-1} D_a \bar{F}_k(\dot{x}(s_0)) \quad \text{for } k \in \{-2, 0, 2\},$$

and $\tilde{v}_k = 0$ for $k \notin \{-2, -1, 0, 1, 2\}$. Next we set $\tilde{v}_{\pm 1}(s_0) = c_{\pm} \hat{v}_{\pm 1}(s_0)$, where

$$\begin{bmatrix} c_- \\ c_+ \end{bmatrix} = -C^{-1} \begin{bmatrix} \langle [q_v^{\mathbb{C}}]_{-2}, \tilde{v}_{-2} \rangle + \langle [q_v^{\mathbb{C}}]_0, \tilde{v}_0 \rangle + \langle [q_v^{\mathbb{C}}]_2, \tilde{v}_2 \rangle \\ \langle [q_v^{\oplus}]_{-2}, \tilde{v}_{-2} \rangle + \langle [q_v^{\oplus}]_0, \tilde{v}_0 \rangle + \langle [q_v^{\oplus}]_2, \tilde{v}_2 \rangle \end{bmatrix},$$

with C defined in (5.10). It is not difficult to check that, by construction, $(\tilde{v}, 0, 1, 0)$ is in the kernel of \mathcal{P} .

We are now ready to state a result for the rigorous verification of Hopf bifurcations.

Proposition 5.4. *Assume*

$$(\hat{\mu}_0^{[1]})_j + \hat{r} < 0, \quad \text{and} \quad (\hat{\mu}_1^{[1]})_j - \hat{r} > 0, \quad (5.11a)$$

$$\min\left\{(\hat{\mu}_0^{[2]})_j, (\hat{\mu}_1^{[2]})_j\right\} - \hat{r} > 0, \quad (5.11b)$$

$$(\hat{\alpha}_0^{[0]})_j + \hat{r} < 0, \quad \text{and} \quad (\hat{\alpha}_1^{[0]})_j - \hat{r} > 0. \quad (5.11c)$$

Then the solutions curve $\hat{x}(s)$ goes through a unique nondegenerate Hopf bifurcation (folding to the right) with respect to μ in the interval $s \in [0, 1]$.

Proof. The proof follows the same lines as the one of Proposition 3.7, and we comment only on the additional steps. Assumptions (5.11a) and (5.11b) imply that there is a unique $s_{\star} \in (0, 1)$ such that $\hat{\mu}'(s_{\star}) = 0$. Assumption (5.11c) implies that there is a $s_0 \in (0, 1)$ such that $\hat{a}(s_0) = 0$. The analysis of the kernel of the operator \mathcal{P} above shows that $\hat{\mu}'(s_0) = 0$. Hence the unique nondegenerate fold with respect to μ occurs at $s_{\star} = s_0$.

For $s \neq s_{\star}$ we have $\hat{a}(s) \neq 0$, since the analysis above shows that $\hat{a}(s) = 0$ implies $\hat{\mu}'(s) = 0$, which occurs at $s = s_{\star}$ only. The amplitude condition (5.4) then guarantees that for $s \neq s_{\star}$ the solution $\hat{u}(t; s)$, represented in Fourier space by $\hat{y}(s) + \hat{a}(s)\hat{v}(s)$, is not time-independent.

Finally, it follows from Remark 5.3 that $D_u f(\hat{y}(s_{\star}), \hat{\mu}(s_{\star}))$ is invertible, hence by the implicit function theorem $\hat{y}(s_{\star})$ is part of a smooth one parameter family of equilibria $\check{y}(\mu)$ with $\check{y}(\hat{\mu}(s_{\star})) = \hat{y}(s_{\star})$. \square

Remark 5.5. *The conclusion of Proposition 5.4 also holds when the inequalities in the assumptions (5.11c) are reversed. Similarly, when the three inequalities in (5.11a)–(5.11b) are reversed then the result holds with the curve folding to the left.*

Traditionally, a Hopf bifurcation point (rather than the branch of periodic solutions emanating from it) is described in terms conditions on eigenvalues of the Jacobian at the critical point as well as other normal form parameters. Clearly, finding just the Hopf bifurcation point only requires solving the algebraic system (where we have split complex eigenvectors in real and imaginary parts, and $\varphi_1, \varphi_2 \in \mathbb{R}^n$)

$$\begin{bmatrix} f(y, \mu) \\ D_u f(y, \mu) y_1 + \beta y_2 \\ D_u f(y, \mu) y_2 - \beta y_1 \\ \varphi_1^T y_1 - \varphi_2^T y_2 - 1 \\ \varphi_2^T y_1 + \varphi_1^T y_2 \end{bmatrix} = 0, \quad \text{with } (y, y_1, y_2, \mu, \beta) \in \mathbb{R}^{3n+2},$$

which can also be attacked using the radii polynomial approach, albeit in the much simpler finite dimensional setting. Obviously, this is how one may locate computationally a Hopf bifurcation point and use it as a numerical starting point for a rigorous continuation of the desingularized problem for the periodic orbits. Additionally, if desired, one may study the eigenvalue problem of the equilibrium ($\varphi_0 \in \mathbb{C}^n$)

$$\mathcal{L}_{\mu}(y, y_0, \gamma) \stackrel{\text{def}}{=} \begin{bmatrix} f(y, \mu) \\ D_u f(y, \mu) y_0 - \gamma y_0 \\ \varphi_0^T y_0 - 1 \end{bmatrix} = 0, \quad \text{with } (y, y_0, \gamma) \in \mathbb{C}^{2n+1}, \mu \in \mathbb{R},$$

for example to determine the algebraic multiplicity of the purely imaginary eigenvalues $i\hat{\tau}(s_\star)^{-1}$ and to confirm that $A_0 = D_u f(\check{y}(\mu_\star), \mu_\star)$ has no other purely imaginary eigenvalues apart from its complex conjugate (the analysis in Fourier space excludes only integer multiples of $\pm i\hat{\tau}(s_\star)^{-1}$). Furthermore, when the algebraic multiplicity of $i\hat{\tau}(s_\star)^{-1}$ is one (as it generically will be) then one may establish the direction in which this eigenvalue moves when μ is varied through $\mu_\star = \hat{\mu}(s_\star)$, by solving the linear system

$$\begin{bmatrix} A_0 & 0 & 0 \\ D_{u,u}^2 f(\check{y}(\mu_\star), \mu_\star) \check{y}_0(\mu_\star) & A_0 - \check{\gamma}(\mu_\star) & -\check{y}_0(\mu_\star) \\ 0 & \varphi_0 & 0 \end{bmatrix} \begin{bmatrix} \check{y}'(\mu_\star) \\ \check{y}'_0(\mu_\star) \\ \check{\gamma}'(\mu_\star) \end{bmatrix} = \begin{bmatrix} D_{\mu} f(\check{y}(\mu_\star), \mu_\star) \\ D_{u,\mu}^2 f(\check{y}(\mu_\star), \mu_\star) \check{y}_0(\mu_\star) \\ 0 \end{bmatrix}.$$

Here the matrix in the lefthand side is invertible when A_0 is invertible and the algebraic multiplicity of $\check{\gamma}(\mu_\star) = i\hat{\tau}(s_\star)^{-1}$ is 1. All these computations are on finite dimensional algebraic systems, and can relatively easily be done in interval arithmetic to ensure that the results are mathematically rigorous.

6 From Hopf bifurcation to global continuation

In the previous sections, we presented an approach to validate Hopf bifurcations and a local family of periodic orbits. In the desingularized Hopf problem (1.6) we solved for \bar{u} and $\bar{\lambda} = (\tau, a, y, \mu)$ instead of u and $\lambda = (\tau, \mu)$. At some distance from the Hopf bifurcation point one would prefer to start working directly with the simpler systems (1.3). Here we discuss how to switch from a solution branch for $(\bar{u}, \bar{\lambda}) = (\bar{u}, (\tau, a, y, \mu))$ to a solution branch for $(u, \lambda) = (u, (\tau, \mu))$. In particular, when we “glue” the end (periodic orbit) point of a continuation step for the desingularized system to the starting (periodic orbit) point of a continuation step for the original system, we want to be sure that the solutions branches connect. We denote the numerical approximations at the boundary points by $(\hat{u}_1, (\hat{\tau}_1, \hat{a}_1, \hat{y}_1, \hat{\mu}_1))$ and $(\hat{u}_0, (\hat{\tau}_0, \hat{\mu}_0))$, respectively, and for natural reasons we choose to set

$$\hat{\tau}_0 = \hat{\tau}_1 \quad \text{and} \quad \hat{\mu}_0 = \hat{\mu}_1 \quad \text{and} \quad \hat{u}_0 = \hat{y}_1 + \hat{a}_1 \hat{u}_1. \quad (6.1)$$

The solutions found at the boundary points are denoted by $(\hat{u}_1, (\hat{\tau}_1, \hat{a}_1, \hat{y}_1, \hat{\mu}_1))$ and $(\hat{u}_0, (\hat{\tau}_0, \hat{\mu}_0))$. For the solutions curves to glue nicely we need to check that

$$\hat{\tau}_0 = \hat{\tau}_1 \quad \text{and} \quad \hat{\mu}_0 = \hat{\mu}_1 \quad \text{and} \quad \hat{u}_0 = \hat{y}_1 + \hat{a}_1 \hat{u}_1. \quad (6.2)$$

The main technical issue lies in lining up the phase condition and continuation equation at the boundary points. There is considerable freedom in choosing these equations, and we will make use of that. In what follows we will switch from a function u to its Fourier components v without further ado.

We note that the coordinate transformation

$$u = y + a\bar{u} \quad (6.3)$$

is essentially a nonlinear change of variables, since a is part of the set of unknowns. On the other hand, in terms of Fourier coefficients the transformation is relatively simple: all modes get rescaled by the same scalar a and only in the 0-th mode the vector y is added. Let us denote the phase condition at the starting point of the continuation step in the original problem by

$$\langle q_0^{\mathbb{C}}, x \rangle = 0, \quad \text{where } q_0^{\mathbb{C}} = (q_{0v}^{\mathbb{C}}, 0).$$

Here we assume the 0-th Fourier component of $q_{0v}^{\mathbb{C}}$ to vanish, see also (2.8). In view of the action of the transformation (6.3) on the Fourier coefficients, as discussed above, it transforms (6.5) into an *equivalent* condition in desingularized coordinates of the form

$$\langle \bar{q}_1^{\mathbb{C}}, \bar{x} \rangle = 0, \quad \text{where } \bar{q}_1^{\mathbb{C}} = (\bar{q}_{1v}^{\mathbb{C}}, 0) \quad \text{with } \bar{q}_{1v}^{\mathbb{C}} = \hat{a}_1 q_{0v}^{\mathbb{C}}, \quad (6.4)$$

provided $\hat{a}_1 \neq 0$. Other rescalings work as well; this particular one is inspired by (2.8). Hence we choose (6.4) as the phase condition at the end of the continuation step in the desingularized problem, i.e. $\hat{q}_{1v}^{\mathcal{C}} = \hat{a}_1 q_{0v}^{\mathcal{C}}$. In essence, this guarantees that the phase of the solution does not shift at the transition.

Next, we follow a similar reasoning for the continuation equation. Let us denote the continuation equation at the starting point of the continuation step in the original problem by

$$\langle q_0^{\circ}, x \rangle = \langle q_0^{\circ}, \hat{x}_0 \rangle. \quad (6.5)$$

In general the transformed condition in desingularized coordinates is *not* affine linear. In principle, this is not a problem for the continuation method. The restriction to affine linear conditions was only made for simplicity of presentation in the current paper. Preferring to stay in this affine linear context for consistency, we simply require $q_0^{\circ} = (q_{0v}^{\circ}, q_{0\lambda}^{\circ})$ to have nonvanishing λ -components only, i.e. $q_0^{\circ} = (0, q_{0\lambda}^{\circ}) = (0, (q_{0\tau}^{\circ}, q_{0\mu}^{\circ}))$. This essentially corresponds to parameter continuation rather than pseudo-arclength continuation at this gluing step. For this choice, the corresponding equivalent condition for the desingularized problem is

$$\langle \bar{q}_1^{\circ}, \bar{x} \rangle = \langle \bar{q}_1^{\circ}, \hat{\bar{x}}_0 \rangle, \quad \text{where } \bar{q}_1^{\circ} = (0, (q_{0\tau}^{\circ}, 0, 0, q_{0\mu}^{\circ})). \quad (6.6)$$

Assuming parameter continuation at the transition point requires us to “force” the continuation code to switch away from the preferable pseudo-arclength continuation in the neighborhood of the gluing point. Nevertheless, this can be implemented in a relatively straightforward manner.

With the choices (6.4) and (6.6) for the phase and continuation equations, it is not difficult to establish that $(\hat{y}_1 + \hat{a}_1 \hat{u}_1, (\hat{\tau}_1, \hat{\mu}_1))$ is a solution to the problem at the starting point of the continuation step for the original system. It remains to establish that it is the same solution as $(\hat{u}_0, (\hat{\tau}_0, \hat{\mu}_0))$. For this final step we use the uniqueness result in Theorem 2.5. Let the balls used to prove the end and starting points be denoted by $B_1 = B_{\hat{r}_1}(\hat{v}_1, \hat{\lambda}_1)$ and $B_0 = B_{\hat{r}_0}(\hat{v}_0, \hat{\lambda}_0)$, respectively. If the transformed ball

$$B_{1 \rightarrow 0} \stackrel{\text{def}}{=} \{(y + av, (\tau, \mu)) : (v, (\tau, a, y, \mu)) \in B_1\}$$

and the ball B_0 are nested, then by uniqueness of the solutions in B_1 and B_0 we conclude that indeed (6.2) hold, see also [3, 26] for similar arguments. Since the centers of the balls are equivalent in view of (6.1), to guarantee the inclusion $B_{1 \rightarrow 0} \subset B_0$ it suffices to check that

$$\left(1 + |\hat{a}_1| + \max_{1 \leq j \leq n} \|(\hat{v}_1)_j\|_{\nu} + \hat{r}_1\right) \hat{r}_1 < \hat{r}_0. \quad (6.7)$$

Indeed, let

$$(v, (\tau, a, y, \mu)) = (\hat{v}_1, (\hat{\tau}_1, \hat{a}_1, \hat{y}_1, \hat{\mu}_1)) + \hat{r}_1(x_v, (x_{\tau}, x_a, x_y, x_{\mu}))$$

with

$$\max_{1 \leq j \leq n} \|(x_v)_j\|_{\nu} \leq 1, \quad |x_{\tau}| \leq 1, \quad |x_a| \leq 1, \quad \max_{1 \leq j \leq n} |(x_y)_j| \leq 1, \quad |x_{\mu}| \leq 1, \quad (6.8)$$

represent any element in B_1 . Then in view of (6.1) we have

$$(y + av, (\tau, \mu)) - (\hat{v}_0, (\hat{\tau}_0, \hat{\mu}_0)) = (\hat{r}_1 x_y + \hat{r}_1 \hat{a}_1 x_v + \hat{r}_1 x_a \hat{v}_1 + \hat{r}_1^2 x_a x_v, (\hat{r}_1 x_{\tau}, \hat{r}_1 x_{\mu})).$$

The bounds (6.8) imply that to check that $B_{1 \rightarrow 0} \subset B_0$ we require $\hat{r}_1 \leq \hat{r}_0$, which follows from (6.7), as well as, for any $j = 1, \dots, n$,

$$\begin{aligned} & \|\hat{r}_1(x_y)_j + \hat{r}_1 \hat{a}_1(x_v)_j + \hat{r}_1 x_a(\hat{v}_1)_j + \hat{r}_1^2 x_a(x_v)_j\|_{\nu} \\ & \leq \hat{r}_1 \|(x_y)_j\|_{\nu} + \hat{r}_1 |\hat{a}_1| \|(x_v)_j\|_{\nu} + \hat{r}_1 |x_a| \|(\hat{v}_1)_j\|_{\nu} + \hat{r}_1^2 |x_a| \|(x_v)_j\|_{\nu} \\ & \leq \hat{r}_1 + \hat{r}_1 |\hat{a}_1| + \hat{r}_1 \|(\hat{v}_1)_j\|_{\nu} + \hat{r}_1^2 \leq \hat{r}_0, \end{aligned}$$

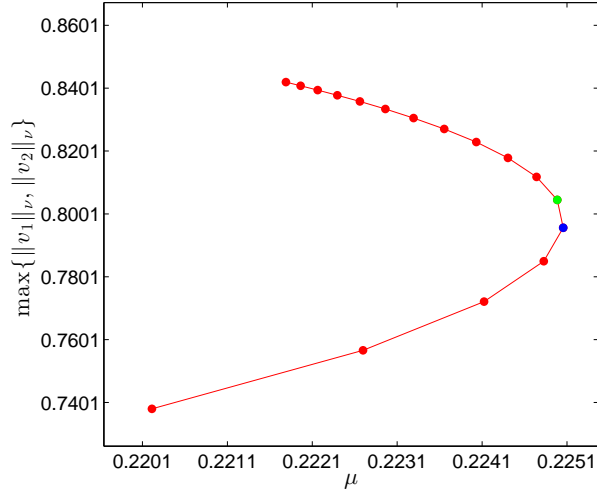


Figure 2: Validated continuation of the branch of periodic solutions in the Rychkov system (7.1). The fold occurs at $\mu_\star \in 0.224955 + [-6.2, 6.2] \cdot 10^{-5}$. The saddle has been validated between the blue and the green dot, but this precision was possible thanks to refinement.

where the final inequality is guaranteed by condition (6.7).

Finally, it is clear from (6.7) that the inclusion $B_{1 \rightarrow 0} \subset B_0$, and hence continuity of the solution branch at the switching point, is more easily established when the radius \hat{r}_1 used to validate the end point of the continuation in desingularized variables is taken as small as possible, while the radius \hat{r}_0 used to validate the starting point of the continuation in the original variables is taken as large as possible.

7 Examples

We present some examples that can be analyzed with the material presented in this paper, which provides a robust and flexible method for identifying and validating fold and Hopf bifurcations in systems of ODEs. The first example is the saddle-node validation in the so-called Rychkov system. This is followed by three examples of Hopf bifurcations, including a Hamiltonian problem in Section 7.4.

7.1 The fold in the Rychkov system

The Rychkov system, first presented in [23], is given by

$$\begin{cases} \dot{u}_1 = u_2 - u_1^5 + u_1^3 + \mu u_1 \\ \dot{u}_2 = -u_1. \end{cases} \quad (7.1)$$

It was proven in [10] to have no periodic solutions for $\mu > 0.2249654$ and two periodic solutions for $\mu < 0.224$. Additionally, it was shown in [10] that the curve of periodic orbits undergoes a saddle-node bifurcation for some μ in the interval $[0.224, 0.2249654]$. Here we locate the bifurcation point more precisely, and we prove that a *nondegenerate* fold occurs.

We start our validated continuation at $\mu = 0.2245$ and continue the periodic solution for increasing μ . In Figure 2 we plot the norm $\max\{\|v_1\|_\nu, \|v_2\|_\nu\}$ of the Fourier series of the periodic orbit versus the

parameter μ . During the continuation, we test numerically for the existence of a saddle-node, and when a numerical indication is found for the occurrence of a fold, then we validate the numerically found saddle-node using Proposition 3.7. We find that a nondegenerate fold is located at

$$\mu_* \in 0.224955 + [-6.2, 6.2] \cdot 10^{-5}.$$

For the validation of the fold, we set $\nu = 1.01$ and the code (heuristically) selects the dimension of finite dimensional projection to be $K = 44$.

The corresponding MATLAB code, available at [27], is provided in `figure_rychkov_saddle.m`.

7.2 A Hopf bifurcation in an extended Lorenz-84 model

The extended Lorenz-84 model

$$\begin{cases} \dot{u}_1 = -u_2^2 - u_3^2 - au_1 - af - bu_4^2 \\ \dot{u}_2 = u_1u_2 - cu_1u_3 - u_2 + d \\ \dot{u}_3 = cu_1u_2 + u_1u_3 - u_3 \\ \dot{u}_4 = -eu_4 + bu_4u_1 + \mu \end{cases} \quad (7.2)$$

is a four dimensional system of ODEs with 7 parameters, see [14, Section 3.1] and [15, Section 4.2]. Inspired by the parameter choices in those papers, we fix

$$a = 0.25, \quad b = 0.987, \quad c = 1, \quad d = 0.25, \quad e = 1.04, \quad f = 2, \quad (7.3)$$

and consider μ as the bifurcation parameter. The system undergoes two Hopf bifurcations at $\mu \approx 0.05$ and $\mu \approx 0.01$.

Applying the approach presented in Section 5, we proved the existence of a Hopf bifurcation at

$$\mu^* \in 0.05684121 + [-9.1, 9.1] \cdot 10^{-6},$$

by using the computational parameters $K = 5$ and $\nu = 1.1$. The eigenvalue crossing the imaginary axis is $-0.5300219i + i[-4.6, 4.6] \cdot 10^{-5}$. The (normalized) period of the solution at the Hopf bifurcation is $\tau = -1.886714 + [-1.6, 1.6] \cdot 10^{-4}$. The periodic orbits bifurcates from the equilibrium $[1.197556, -0.033525, 0.203229, -0.400337] + [-1.6, 1.6] \cdot 10^{-4}$.

Additionally, in the framework of the desingularized Hopf system we continued the periodic orbit and the fixed point solution up to $\mu \approx -0.0023$, where the periodic solution has an amplitude $a \approx 0.9394$. In Figure 3, we plotted the desingularized (“blown up”) periodic solution \bar{u} near the Hopf bifurcation (where it is unimodal) and at the end of the continuation.

The stepsize, that is, the distance between consecutive numerical approximate solutions $\|\hat{x}_0 - \hat{x}_1\|_X$ used in Figure 3 was relatively large: $h = 10^{-3}$. The (refined) step where the Hopf bifurcation is proven to take place goes from amplitude $a = 4.6671 \cdot 10^{-6} + [-8.1, 8.1] \cdot 10^{-8}$ to $a = -5.62556 \cdot 10^{-5} + [-8.1, 8.1] \cdot 10^{-8}$. We can increase the accuracy of locating the Hopf bifurcation point by adopting a smaller stepsize and/or increasing the number of modes used. With $h = 10^{-3}$ and $K = 10$, we find

$$\mu^* \in 0.05684121 + [-6.3, 6.3] \cdot 10^{-6},$$

which reflects a modest improvement. However, with $h = 10^{-5}$ and $K = 10$, we retrieve a much higher accuracy result:

$$\mu^* \in 0.056841207164 + [-4.4, 4.4] \cdot 10^{-10}.$$

We conclude that decreasing the stepsize is the crucial factor in improving accuracy, whereas the number of modes used is less important, as may be expected since the solution is unimodal at $a = 0$.

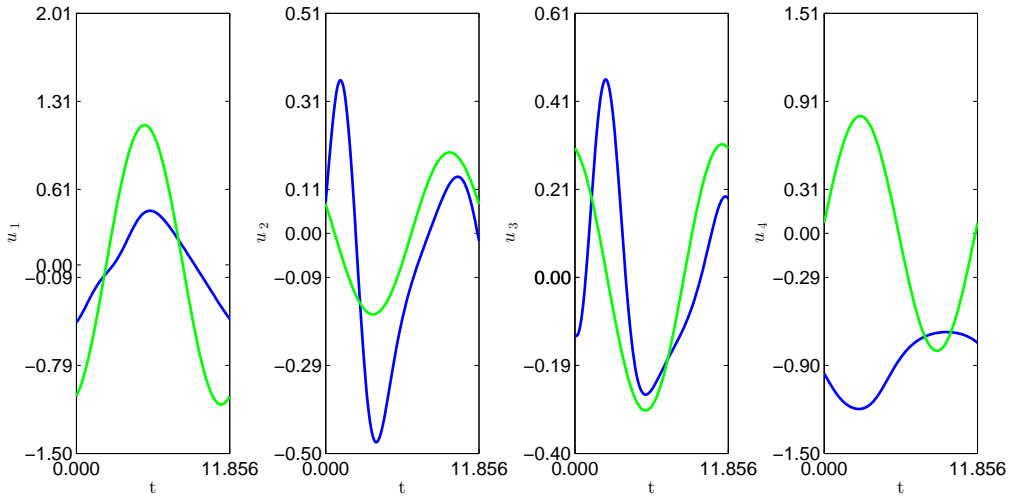


Figure 3: The four components of the desingularized periodic solution \bar{u} corresponding to the extended Lorenz-84 system (7.2), in green for $\mu \approx 0.056$ very close to the Hopf bifurcation, and in blue for $\mu \approx -0.0042$ further away from it. The code automatically adds modes when needed; the final (blue) solution has been validated with $K = 53$. The continuous branch connecting the two solutions has been validated. The horizontal axis represents time in the original system.

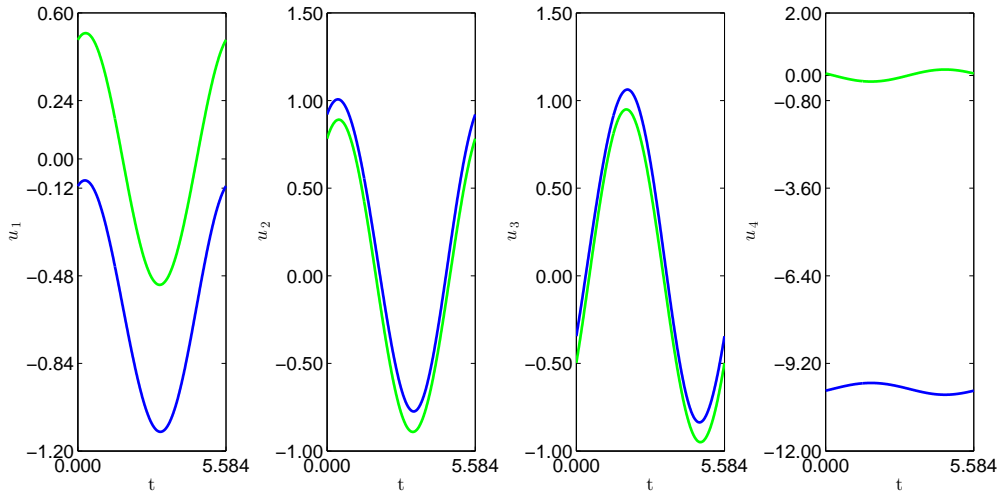


Figure 4: The four components of the desingularized periodic solution \bar{u} corresponding to the extended Lorenz-84 system (7.2), in green for $\mu \approx 0.0109$ close to the Hopf bifurcation, and in blue for $\mu \approx -0.0108$ further away from it. The continuous branch connecting the two solutions has been validated. The horizontal axis represents time in the original system.

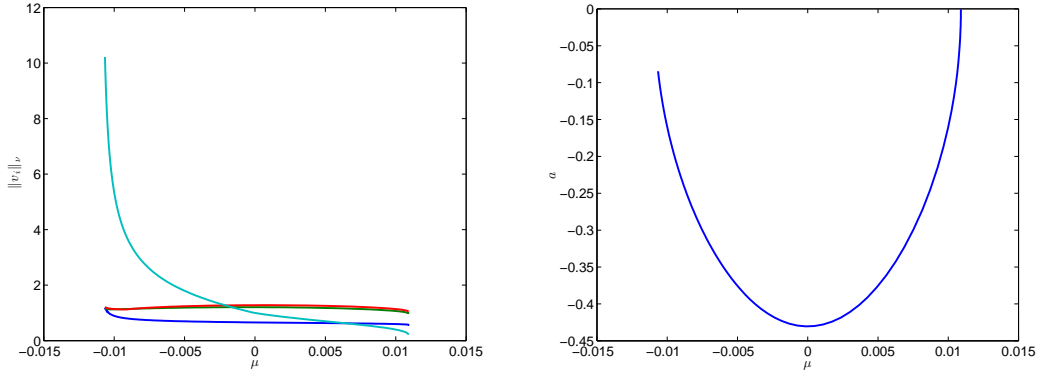


Figure 5: In the left graph the norms $\|v_i\|_\nu$, $i = 1, 2, 3, 4$ of the components of the solution branch presented in Figure 4 are plotted with respect to the parameter μ . On the right, the amplitude a of the desingularized orbit is plotted with respect to the parameter μ .

The second Hopf bifurcation for the same values of the parameters (7.3) takes place at

$$\mu \in 0.010900160 + [-3.1, 3.1] \cdot 10^{-7}.$$

The stationary solution is at $[1.079797955, -0.017016937, 0.230267229, -0.423161664] + [-3.1, 3.1] \cdot 10^{-7}$, while the eigenvalue crossing the imaginary axes is $1.1251599i + i[-1.6, 1.6] \cdot 10^{-5}$. The period of the periodic perturbation near the Hopf bifurcation is $\tau = 0.888763098 + [-3.1, 3.1] \cdot 10^{-7}$. In Figure 4, we depict the desingularized periodic solution \bar{u} near the Hopf bifurcation (where it is unimodal) and after 800 continuation steps, where

$$\mu \in -0.0108027 + [-6.3, 6.3] \cdot 10^{-5}.$$

In Figure 5, the norm of the periodic orbit is plotted along the branch with respect to the parameter μ . We conclude from the fact that a approaches zero at both ends of the branch, while the norms $\|v_i\|_\nu$ of the rescaled time-dependent part \bar{u} explode at one end point, that the continuous branch of periodic solutions that originates from a Hopf point at $\mu \approx 0.0109$ terminates for $\mu \approx -0.0108$ at another Hopf point on a different branch of equilibria, not connected by continuation.

In Figure 1 we depict a full continuous branch of periodic orbits of (7.2), connecting these two Hopf bifurcation points. The periodic orbits “cross over” from one branch of equilibria to another. Hence we use the gluing approach discussed above twice, first to switch from the desingularized system around one equilibrium to continuation of the original system, and once more to switch from the original system to the desingularized system around the other equilibrium.

The corresponding MATLAB code is provided in `lorenz84_validated_cont.m`.

7.3 A Hopf bifurcation in a hyperchaotic system

In [20], the 4-dimensional (hyperchaotic) ODE system

$$\begin{cases} \dot{u}_1 = a(u_1 - u_2) + u_2 u_3 + u_4 \\ \dot{u}_2 = -b u_2 + u_1 u_3 \\ \dot{u}_3 = -c u_3 + d u_1 + u_1 u_2 \\ \dot{u}_4 = -e(u_1 + u_2) \end{cases} \quad (7.4)$$

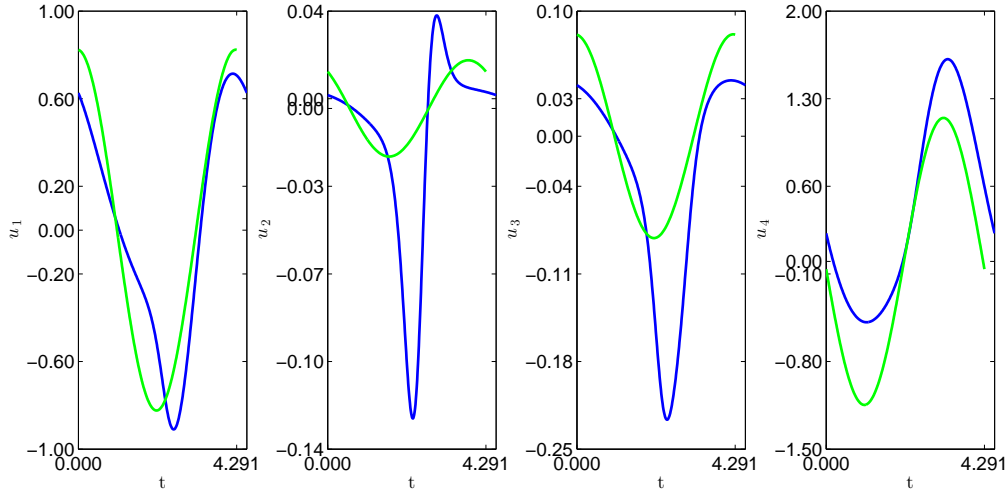


Figure 6: The four components of the desingularized periodic solution \bar{u} corresponding to the 4-dimensional hyperchaotic system (7.4), in green for $\mu = -1.0155$ close to the Hopf bifurcation, and in blue for $\mu \approx -1.7035$ further away from it. The continuous branch connecting the two solutions has been validated. The horizontal axis represents time in the original system.

is presented and studied. The system has many interesting dynamic features, including Hopf bifurcations. Inspired by the analysis in [20] we fix

$$b = c = 1, \quad d = 10, \quad e = 2,$$

and use $\mu = a$ as the bifurcation parameter. Then, a Hopf bifurcation occurs at

$$\mu_* \in -1.01551372619 + [-2.5, 2.5] \cdot 10^{-9},$$

from the equilibrium

$$(u_1, u_2, u_3, u_4) \in (10.09901951359, -10.09901951359, -1.00000000000, 30.61040538783) + [-2.5, 2.5] \cdot 10^{-9},$$

where the interval notation has been slightly abused. The normalized period at the Hopf bifurcation is $\hat{\tau}(s_*) \in 0.68299909941 + [-2.5, 2.5] \cdot 10^{-9}$. We continued the solution to $\mu \approx -1.043$, where the amplitude $a \approx 2.149$. In Figure 6 we have depicted the desingularized periodic profile \bar{u} . For this validation we used $K = 15$ and $\nu = 1.1$. The corresponding MATLAB code is provided in `main_hyper.m`.

7.4 A Hamiltonian example

Consider the fourth order parabolic partial differential equation (PDE)

$$u_t = -u_{xxxx} + au_{xx} + bu + cu^2 + du^3. \quad (7.5)$$

This family includes the extended Fisher-Kolmogorov and Swift-Hohenberg equations (see [22] and the references therein). When studying stationary states for the problem with periodic or Neumann boundary conditions, this reduces to studying periodic solutions of the ODE

$$u_{xxxx} = au_{xx} + bu + cu^2 + du^3. \quad (7.6)$$

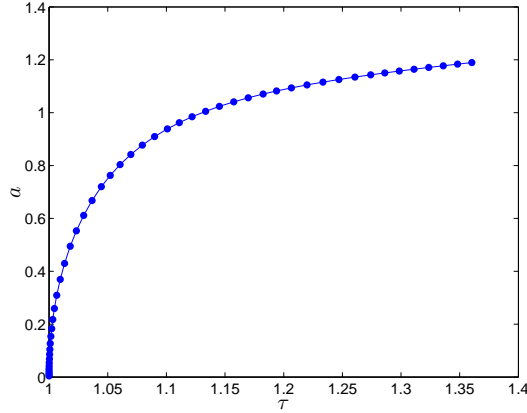


Figure 7: The Hopf bifurcation, or fold for the desingularized system, with respect to the normalized period τ , for (7.8) or, equivalently, (7.6).

Even though it clashes with the notation elsewhere in the paper, we denote by x the independent variable in the ODE (7.6), because it fits with the PDE (7.5). This problem is Hamiltonian with conserved quantity

$$E = -u_{xxx}u_x + \frac{1}{2}(u_{xx})^2 + \frac{a}{2}(u_x)^2 + \frac{b}{2}u^2 + \frac{c}{3}u^3 + \frac{d}{4}u^4. \quad (7.7)$$

For any $b > 0$ periodic orbits, which appear in 1-parameter families due to the Hamiltonian structure, bifurcate from the equilibrium $u = 0$ with period $2\pi((a^2/4 + b)^{1/2} - a/2)^{-1/2}$. For the PDE (with periodic or Neumann boundary conditions) this means that nontrivial stationary solutions bifurcate from the trivial state when the domain size is varied. Although this analysis can be done by hand, we use this example to illustrate how Hamiltonian problems can be brought into the framework of the current paper.

We will fix the parameters a, b, c, d and introduce an *artificial* continuation parameter μ to turn (7.6) into the first order system

$$\begin{cases} \dot{u}_1 = u_2 \\ \dot{u}_2 = u_3 \\ \dot{u}_3 = u_4 \\ \dot{u}_4 = au_3 + bu_1 + cu_1^2 + du_1^3 + \mu u_2. \end{cases} \quad (7.8)$$

Irrespective of μ , the equilibria of the system are $u_2 = u_3 = u_4 = 0$ and u_1 a zero of the polynomial $p(u) = bu + cu^2 + du^3$, which also correspond to stationary solutions of (7.6). Furthermore, we know *a priori* that $\mu = 0$ for any periodic solution of (7.8), since (cf. (7.7))

$$0 = \int_0^L \frac{d}{dx} \left(-u_4u_2 + \frac{1}{2}u_3^2 + \frac{a}{2}u_2^2 + \frac{b}{2}u_1^2 + \frac{c}{3}u_1^3 + \frac{d}{4}u_1^4 \right) dx = -\mu \int_0^L u_2^2 dx,$$

where L is the period of the solution. Hence, any periodic orbit of (7.8) corresponds to a periodic solution of (7.6) (and vice versa). The advantage of studying (7.8) rather than (7.6) is that in the former the Hamiltonian structure/symmetry has been broken, and we can study it using the general continuation and bifurcation techniques from this paper.

In Figure 7, the validated bifurcation is shown for the parameters $a = 2$, $b = 3$, $c = 1$, $d = -1$. The location of the bifurcation point $\hat{\tau}(s_*)$ is validated to lie in $1 + [0.4, 0.4] \cdot 10^{-4}$ using computational

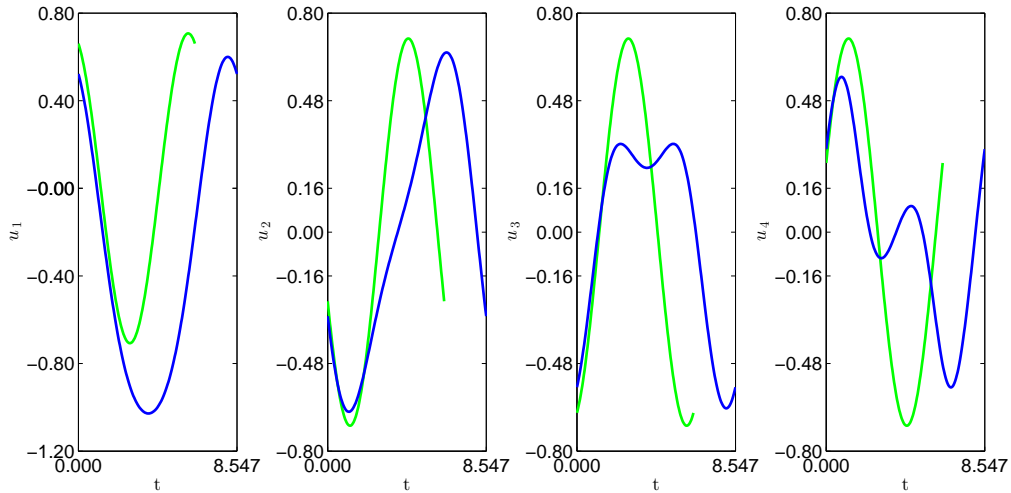


Figure 8: The four components of the desingularized periodic solution \bar{u} corresponding to (7.8), in green for $\tau = 1$ very close to the Hopf bifurcation, and in blue for $\tau \approx 1.224$ further away from it. The continuous branch connecting the two solutions has been validated. The horizontal axis represents time in the original system.

parameters $K = 5$ and $\nu = 1.1$ (as discussed, it is analytically determined to occur at $\lambda_1 = \tau = 1$). Desingularized profiles are plotted in Figure 8, continued from $\tau = 1$ to $\tau \approx 1.224$. The corresponding MATLAB code is provided in `main_Hamiltonian.m`.

References

- [1] G. Arioli and H. Koch. Computer-assisted methods for the study of stationary solutions in dissipative systems, applied to the kuramoto–sivashinski equation. *Archive for rational mechanics and analysis*, 197(3):1033–1051, 2010.
- [2] M. Breden and R. Castelli. Existence and instability of steady states for a triangular cross-diffusion system: a computer-assisted proof. *J. Differential Equations*, 264(10):6418–6458, 2018.
- [3] M. Breden, J.-P. Lessard, and M. Vanicat. Global bifurcation diagrams of steady states of systems of pdes via rigorous numerics: a 3-component reaction-diffusion system. *Acta applicandae mathematicae*, 128(1):113–152, 2013.
- [4] R. Clewley, W. Sherwood, M. LaMar, and J. Guckenheimer. PyDSTool, a software environment for dynamical systems modeling, 2007. <https://sourceforge.net/projects/pydstool/>.
- [5] H. Dankowicz and F. Schilder. *Recipes for continuation*, volume 11 of *Computational Science & Engineering*. Society for Industrial and Applied Mathematics (SIAM), Philadelphia, PA, 2013. <https://sourceforge.net/projects/cocotools/>.
- [6] A. Dhooge, W. Govaerts, Y. A. Kuznetsov, H. G. E. Meijer, and B. Sautois. New features of the software MatCont for bifurcation analysis of dynamical systems. *Math. Comput. Model. Dyn. Syst.*, 14(2):147–175, 2008. <https://sourceforge.net/projects/matcont/>.

- [7] E. Doedel, B. Oldeman, A. Champneys, F. Dercole, T. Fairgrieve, Y. Kuznetsov, R. Paffenroth, B. Sandstede, X. Wang, and C. Zhang. AUTO-07p: Continuation and bifurcation software for ordinary differential equations, 2012. <http://sourceforge.net/projects/auto-07p/>.
- [8] B. Ermentrout. *Simulating, analyzing, and animating dynamical systems*, volume 14 of *Software, Environments, and Tools*. Society for Industrial and Applied Mathematics (SIAM), Philadelphia, PA, 2002. A guide to XPPAUT for researchers and students. <http://www.math.pitt.edu/~bard/xpp/xpp.html>.
- [9] M. Gameiro, J.-P. Lessard, and A. Pugliese. Computation of smooth manifolds via rigorous multi-parameter continuation in infinite dimensions. *Found. Comput. Math.*, 16(2):531–575, 2016.
- [10] A. Gasull, H. Giacomini, and M. Grau. Effective construction of Poincaré-Bendixson regions. *J. Appl. Anal. Comput.*, 7(4):1549–1569, 2017.
- [11] Y. Kanzawa and S. Oishi. Calculating bifurcation points with guaranteed accuracy. *IEICE Trans. Fundamentals E82-A 6*, pages 1055–1061, 1999.
- [12] D. E. Knuth. *The art of computer programming. Vol. 2*. Addison-Wesley Publishing Co., Reading, Mass., second edition, 1981. Seminumerical algorithms, Addison-Wesley Series in Computer Science and Information Processing.
- [13] H. Kokubu, D. Wilczak, and P. Zgliczyński. Rigorous verification of cocoon bifurcations in the Michelson system. *Nonlinearity*, 20(9):2147–2174, 2007.
- [14] Y. A. Kuznetsov, H. G. E. Meijer, W. Govaerts, and B. Sautois. Switching to nonhyperbolic cycles from codim 2 bifurcations of equilibria in ODEs. *Phys. D*, 237(23):3061–3068, 2008.
- [15] Y. A. Kuznetsov, H. G. E. Meijer, and L. van Veen. The fold-flip bifurcation. *Internat. J. Bifur. Chaos Appl. Sci. Engrg.*, 14(7):2253–2282, 2004.
- [16] J.-P. Lessard. Recent advances about the uniqueness of the slowly oscillating periodic solutions of Wright’s equation. *J. Differential Equations*, 248(5):992–1016, 2010.
- [17] J.-P. Lessard. Rigorous verification of saddle-node bifurcations in ODEs. *Indag. Math. (N.S.)*, 27(4):1013–1026, 2016.
- [18] J.-P. Lessard, J. D. Mireles James, and J. Ransford. Automatic differentiation for Fourier series and the radii polynomial approach. *Phys. D*, 334:174–186, 2016.
- [19] J.-P. Lessard, E. Sander, and T. Wanner. Rigorous continuation of bifurcation points in the diblock copolymer equation. *J. Comput. Dyn.*, 4(1-2):71–118, 2017.
- [20] X. Li and Z.-Y. Yan. Hopf bifurcation in a new four-dimensional hyperchaotic system. *Commun. Theor. Phys.*, 64(2):197–202, 2015.
- [21] T. Minamoto and M. T. Nakao. Numerical method for verifying the existence and local uniqueness of a double turning point for a radially symmetric solution of the perturbed Gelfand equation. *J. Comput. Appl. Math.*, 202(2):177–185, 2007.
- [22] L. A. Peletier and W. C. Troy. *Spatial patterns*, volume 45 of *Progress in Nonlinear Differential Equations and their Applications*. Birkhäuser Boston, Inc., Boston, MA, 2001. Higher order models in physics and mechanics.
- [23] G. Rychkov. The maximum number of limit cycles of polynomial liénard systems of degree five is equal to two. *Differential Equations*, 11:301–302, 1975.

- [24] K. Tanaka, S. Murashige, and S. Oishi. On necessary and sufficient conditions for numerical verification of double turning points. *Numer. Math.*, 97(3):537–554, 2004.
- [25] J. B. van den Berg and J. Jaquette. A proof of Wright’s conjecture. *J. Differential Equations*, 264(12):7412–7462, 2018.
- [26] J. B. van den Berg, J.-P. Lessard, and K. Mischaikow. Global smooth solution curves using rigorous branch following. *Math. Comp.*, 79(271):1565–1584, 2010.
- [27] J. B. van den Berg, J.-P. Lessard, and E. Queirolo. MATLAB code for “Rigorous verification of Hopf bifurcations”, 2020. <https://www.math.vu.nl/~janbouwe/code/hopf/>.
- [28] J. B. van den Berg and E. Queirolo. A general approach to validated continuation of periodic orbits in systems of polynomial ODEs. Preprint, 2019.
- [29] J. B. van den Berg and J. F. Williams. Validation of the bifurcation diagram in the 2D Ohta-Kawasaki problem. *Nonlinearity*, 30(4):1584–1638, 2017.
- [30] T. Wanner. Computer-assisted bifurcation diagram validation and applications in materials science. In *Rigorous numerics in dynamics*, volume 74 of *Proc. Sympos. Appl. Math.*, pages 123–174. Amer. Math. Soc., Providence, RI, 2018.
- [31] D. Wilczak and P. Zgliczyński. Period doubling in the Rössler system—a computer assisted proof. *Found. Comput. Math.*, 9(5):611–649, 2009.
- [32] P. Zgliczyński. Steady state bifurcations for the Kuramoto-Sivashinsky equation: a computer assisted proof. *J. Comput. Dyn.*, 2(1):95–142, 2015.